STABILITY OF NUCLEATION SITES IN POOL BOILING

by

H. S. RANGANATH

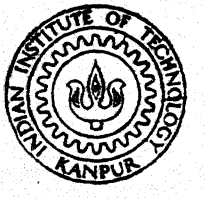

DEPARTMENT OF MECHANICAL ENGINEERING

INDIAN INSTITUTE OF TECHNOLOGY KANPUR

JULY, 1986

STABILITY OF NUCLEATION SITES IN POOL BOILING

A Thesis Submitted

in Partial Fulfilment of the Requirements

for the Degree of

MASTER OF TECHNOLOGY

by

H. S. RANGANATH

to the

DEPARTMENT OF MECHANICAL ENGINEERING

INDIAN INSTITUTE OF TECHNOLOGY KANPUR

JULY, 1986

CERTIFICATE

This is to certify that the work entitled, " Stability of Nucleation Sites in Pool Boiling" by H.S. Ranganath has been carried out under my supervision and has not been submitted elsewhere for the award of a degree.

July, 1986

Keshav Kant

(Dr. Keshav Kant)
Assistant Professor
Department of Mechanical Engineering
Indian Institute of Technology
Kanpur

TO MY

PARENTS

CONTENTS

ABSTRACT

Based upon the bubble nucleation and site deactivation mechanisms proposed by Kant, a dynamic model was developed to study the stability of nucleation sites in the heterogeneous pool boiling of liquids on a single in a natural heated surface. This model predicted the waiting time of a bubble for given boiling conditions in agreement with the available experimental data. The results showed that the diameter and the depth of the nucleation site actually determined the stability and other parameters in pool boiling were not important.

An equation was developed for determining the thickness of the thermal layer on a heated surface. Computed values of the thickness were found to be in agreement with the values available in literature for water and pentane.

Static single bubble nucleation model of Kant was extended to incorporate a generalised temperature distribution for the thermal layer, proposed here. This model was used to predict the nucleation superheats and the size range of active sites on a surface. The results obtained were better than those of other authors.

NOMENCLATURE

a, A_h ... $a_0, a_1, \ldots a_4$	Constants
A_i, A_{im}	Area of l-v interface inside and outside the cavity, m^2
A_{wli_1}, A_{wli_2}	Inside surface areas of cavity wall in contact with liquid in ULCV and LLCV, m^2
B	Constant
C, C_1, C_2, C_a, C_b	Constants
C_c, C_e	Coefficients of contraction and expansion
c_1	Specific heat, J kg^{-1} K^{-1}
C_{sf}	Constant depending upon surface-liquid combination
d	Constant
D_c	Cavity diameter, m
g	Acceleration due to gravity, m s^{-2}
h	Convective heat transfer coefficient, W $m^{-2}K^{-1}$
H	Bubble height, m
h_{fg}	Enthelpy of vaporization, J kg^{-1}
h_i, h_{ic}, h_{ie}	Theoretical and adjusted values of convective heat transfer coefficient for the l-v interface within th cavity, W m^{-2} K^{-1}
h'_{ic}	Convective heat transfer coefficient for the l-v interface excluding the sensible heat of the condensate, W m^{-2} K^{-1}
h_{1c}, h_{1e}	Head loss due to sudden contraction and expansion, m

h_w, h_{wli}	Theoretical and adjusted values of convective wall heat transfer coefficients, W m^{-2} K^{-1}
J	Mechanical equivalent of heat, N m J^{-1}
Ja	Jakob number = $(\rho_1 c_1 / \rho_v h_{fg}) \Delta T$
k, k_{1r}	Thermal conductivity of the liquid and reference liquid, W m^{-1} K^{-1}
L	Cavity depth, m
M	Molecular weight, Kg mol^{-1}
$\dot{m}$	Mass flow rates, Kg s^{-1}
M_1, M_2, M_{2r}	Multipliers
M_1, M_v	Mass within control volumes, Kg
n	Constant
p_c	Critical pressure, Pa
p_{1_i} (i=0,1,..,4)	Liquid pressures, Fig. 4.2, N m^{-2}
p_v	Vapor pressure, N m^{-2}
Q_1, Q_2	Net rates of heat transfer over the bubble surface, W
$\dot{q}$	Heat flux, W m^{-2}
q_{ic}	Rate of condensation heat transfer across -v interface, W
r	Radius, m
R	Universal gas constant 8314.34 J $Kmol^{-1}$ K^{-1}
R_1, R_2	Principal radii of curvature, m
R_b, R_c, R_i	Radii of bubble, cavity and l-v interface, m
S	Height of spherical cap shaped l-v interface, m
S_R	Surface roughness, m

t	Time, s
T	Temperature, K
T_e	Equilibrium vapor temperature, K
t_g	Growth time, s
T_s	Saturation temperature, K
t_w	Waiting time, s
u	Specific internal energy, J Kg^{-1}
V	Average flow velocity in the cavity, m s^{-1}
V_b, V_c	Molal volume and critical volume, cm^3 $g\text{-}mol^{-1}$
VISB, VISTO	Constants
V_m	Mean velocity at the end of a phase, m s^{-1}
V_{sc}	Volume of spherical cap, m^3
y	Distance in Fig. 3.1, m
z	Distance measured from the heating surface into the cavity, m

GREEK LETTERS

α	thermal diffusivity, $m^2\ s^{-1}$
β	shape angle, rad
δ_e	distance from surface where $T = T_e$, m
δ_t	thermal layer thickness, m
ΔT	superheat, K
ΔT_n	nucleation superheat, K
$\varepsilon_1, \varepsilon_2, \varepsilon_3, \varepsilon_4$	indices in equation (3.7)
η	ratio defined in equation (3.14b)
Θ	dynamic contact angle, rad
λ	coefficient of volume expansion, K^{-1}
μ	dynamic viscosity, N s m^{-2}
ν	kinematic viscosity, $m^2\ s^{-1}$
ξ	ratio in equation (3.14b)
$\pi_1, \pi_2 \ldots \pi_8, \pi_2^*, \pi_3^*, \pi_4^*$	dimensionless groups
ρ	density, kg m^{-3}
ρ_c	critical density, kg m^{-3}
σ	surface tension, kg S^{-2}
τ_w	wall shear stress, N m^{-2}
ϕ	angle, rad

Subscripts

b	bulk liquid
c	condensation
e	evaporation
e_1, e_2	first and second evaporation
1	liquid
v	vapor
w	wall
1	ULCV
2	LLCV

ABBREVIATIONS

BP	boiling point
HPB	heterogeneous pool boiling
HP	Hagen-Poiseuille
LLCV	lower liquid control volume
LLVI	lower liquid vapor interface
LTD	linear temperature distribution
l-v	liquid-vapor
MDTD	Marcus Dropkin temperature distribution
NLTD	nonlinear temperature distribution
ODE	ordinary differential equations
ULCV	upper liquid control volume
ULVI	upper liquid vapor interface
VCV	vapor control volume

LIST OF FIGURES

LIST OF TABLES

CHAPTER 1

INTRODUCTION

1.1 POOL BOILING

In a normal pool boiling situation, the surface of the container is usually at a temperature higher than that of the liquid contained therein and this liquid may be at or near its saturation temperature. The heat transfer takes place from the surface to the liquid mostly through a process of phase change of some of the liquid into the vapor state. The applications of such boiling heat transfer are many, not only in apparatuses whose primary purpose is to vaporize a liquid, such as boilers, but also in situations where it is desired to remove heat from a surface at a high rate with the lowest possible surface temperature, such as, nuclear reactors. There are several regimes of pool boiling, like nucleate boiling, transition boiling and film boiling. The most desirable and the important regime is that of nucleate boiling in which bubbles are formed wherever there are nucleation sites such as tiny pits or scratches in the surface. The bubbles transport the latent heat of the phase change and also increase the convective heat transfer by agitating the liquid near the heating surface. Nucleate boiling is essentially a

cyclic process which consists of bubble formation, bubble growth, and its departure. The nucleation sites have to be active or stable for the process to continue. The subject of this thesis is to model the bubble nucleation phenomena to predict the stability of nucleation sites.

Some of the terms used in the following chapters are defined here. Heterogeneous pool boiling refers to the boiling occurring on a surface or on a single cavity in the surface submerged in a pool of liquid. If the liquid is at the boiling point, the term saturated pool boiling is used and if the liquid temperature is lower than its boiling point, the term sub-cooled pool boiling is used. There is a small layer of liquid adjacent to the boiling surface, called the thermal layer, in which most of the temperature drop occurs from the surface temperature to the bulk liquid temperature.

1.2 OBJECTIVES

1. Develop a general equation for the thermal layer thickness.
2. Propose a generalized temperature distribution within the thermal layer and predict nucleation superheats.
3. Develop an expression to predict the size range of active site on a surface.

4. Develop a dynamic single bubble nucleation model for the heterogeneous pool boiling (HPB) of a liquid to predict the minimum wall superheats for the stability of nucleation sites in a surface.

1.3 ORGANISATION OF THE THESIS

Chapter 2 gives the general background of the subject and summarizes all the equations which are used later in the text. Chapter 3 gives the expression for the thermal layer thickness and those for the generalized temperature distribution within the thermal layer and the size range of active nucleation sites. The results obtained are compared with the predictions of other workers. Chapter 4 gives the dynamic single bubble nucleation model for HPB. The predictions of the model are discussed and compared with the predictions and data of other authors. Chapter 5 gives the conclusions followed by references.

CHAPTER 2

GENERAL BACKGROUND

2.1 INTRODUCTION

This chapter deals with the topics that are referred to later on in the thesis. A comprehensive review in Boiling Heat Transfer is not attempted here.

2.2 FUNDAMENTAL EQUATIONS

1. Laplace Equation

For a curved interface, the pressures in the liquid, p_1, and that in the vapor, p_v, are related by the Laplace equation

$$p_v - p_1 = \sigma \left(\frac{1}{R_1} + \frac{1}{R_2}\right) \qquad (2.1)$$

where R_1 and R_2 are the principal radii of curvature of the interface and σ is the surface tension of the liquid. For a spherical interface $R_1 = R_2 = R_i$

$$p_v - p_1 = \frac{2\sigma}{R_i} \qquad (2.2)$$

2. Clausius-Clapeyron Equation

The pressure difference $(p_v - p_1)$ can be related to the equilibrium vapor superheat $(T_e - T_s)$ through this equation and

this relation is given by

$$\frac{dp}{dT} = \frac{h_{fg}\,\rho_v}{T} \qquad (2.3)$$

where ρ_v and h_{fg} represent the density of vapor and enthalpy of vaporization respectively.

Equation (2.3) upon integration along the p-v saturation curve assuming $\frac{\rho_v\, h_{fg}}{T}$ = constant and $T = T_s$ (Rohsenow, 1970), yields

$$T_e - T_s = \frac{2\sigma T_s}{R_i\,\rho_v\,h_{fg}} \qquad (2.4)$$

2.3 THERMAL LAYER THICKNESS

The thermal layer thickness, δ_t, (defined in Section 1.1) plays a very significant role in the case of nucleate boiling. It also plays a very important role in determining the size range of effective nucleation sites. There are some empirical relations available in the literature to estimate the value of δ_t. Most of these relations, relate δ_t to just one or two properties of the liquid like k_1, ν, λ, α and the heat transfer coefficient, h, and are based upon limited and poorly conducted experiments.

Lippert and Dougall (1968) for the pool boiling of water, Freon-113 and Methyl Alcohol showed that the correlations for δ_t could be divided into two distinct regimes. For low heat fluxes ($h \leq 3970$ W $m^{-2}K^{-1}$), for all the three liquids

$$\delta_t = C\, k_1/h \tag{2.5}$$

where k_1 is the thermal conductivity of the boiling liquid and the constant C was taken as 1.65.

For higher heat fluxes the correlation was

$$\delta_t = (C/h)^{1/2.6} \tag{2.6}$$

where the value of C depended on the particular liquid.

According to Marcus and Dropkin (1965), for low heat fluxes ($h \leq 3970$ W m^{-2} K^{-1})

$$\delta_t = 1.57\, k_1/h \tag{2.7}$$

and for high heat fluxes ($h > 3970$ W m^{-2} K^{-1})

$$\delta_t = 0.0177\, h^{-0.5} \text{ metre} \tag{2.8}$$

Han and Griffith (1965) expressed δ_t in terms of the waiting period, t_w as

$$\delta_t = (\pi \alpha t_w)^{1/2} \tag{2.9}$$

where α is the thermal diffusivity of the boiling liquid, and t_w is the waiting time of the bubble (defined in Section 2.5).

For very high wall superheat, where the waiting period is very short, the thickness, δ_t, was given by

$$\delta_t = [\pi\ \alpha(t_w + t_{ub})]^{1/2} \tag{2.10}$$

where t_{ub} is the unbinding period.

As the waiting time increases the thermal layer cannot increase indefinitely. It will be washed off by the natural convection currents of the fluid as it grows beyond the thickness of the natural convection layer, δ_{nc}. This means that the upper bound on δ_t can be written as

$$\delta t_{max} = \delta_{nc} \tag{2.11}$$

The lower bound on δ_t can be determined by using an h value for nucleate boiling from Rohsenows' (1952) correlation

$$\frac{c_1\ (T_w - T_s)}{h_{fg}} = C_{sf}\left[\frac{\dot{q}}{\mu\ h_{fg}}\left\{\frac{\sigma}{g(\rho_1 - \rho_v)}\right\}^{1/2}\right]^{0.33}\left(\frac{c_1\ \mu}{k_1}\right)^{m+1} \tag{2.12}$$

where $\dot{q}$, c_1, μ and C_{sf} represent the heat flux, specific heat, viscosity and a constant for the surface-liquid combination.

Leont'ev and Kirdyashkin (1966) gave the following expression for predicting δ_t,

$$\delta_t = 2.75\left(\frac{\alpha\,\nu}{\Delta T_w\,\lambda g}\right)^{1/3} \tag{2.13}$$

where α, ν and λ represent the thermal diffusivity , kinematic viscosity and coefficient of volume expansion.

2.4 TEMPERATURE DISTRIBUTIONS IN THE THERMAL LAYER

Following temperature distributions (TD) have been suggested for the thermal layer.

1. Linear Temperature Distribution (LTD)

The LTD is given by

$$\frac{T - T_b}{T_w - T_s} = 1 - \frac{y}{\delta_t} \tag{2.14}$$

2. Nonlinear Temperature Distribution (NLTD)

Leont'ev and Kirdyashkin (1966) approximated the TD by the following equation

$$\xi = 1 - 2\eta + 2\eta^3 - \eta^4 \tag{2.15a}$$

where

$$\xi = \frac{T - T_b}{T_w - T_b} \quad \text{and} \quad \eta = \frac{y}{\delta_t} \tag{2.15b}$$

3. Marcus and Dropkin Temperature Distribution (MDTD)

Marcus and Dropkin (1965) suggested the TD as :

$$\frac{T - T_b}{T_w - T_b} = 1 - \frac{y}{\delta_t} \qquad 0 \leq y \leq a\,\delta_t \qquad (2.16a)$$

$$\frac{T - T_b}{T_w - T_b} = d\left(\frac{y}{\delta_t}\right)^{-n} \qquad a\,\delta_t \leq y \leq \delta_t \qquad (2.16b)$$

where a,d and n are constants.

2.5 STATIC BUBBLE NUCLEATION MODELS IN HPB

The presence of thermal layer on a surface makes the predictions of incipient wall superheats difficult, compared to a situation where the boiling liquid is uniformly superheated. The latter situation corresponds to $\delta_t = \infty$.

As mentioned earlier, the formation of a bubble is a cyclic process, the time period between the departures of two successive bubbles is the total period of the bubble cycle. This period is comprised of two periods, namely, the waiting period, t_w, and the growth period, t_g. As the names imply, the former refers to that period during which conditions of heating are reset to produce a visible vapor nucleus on a cavity in the surface following the bubble departure. The latter, i.e., t_g, refers to the period during which the above mentioned visible nucleus grows to its maximum departure size. The reciprocal of $(t_w + t_g)$ gives the frequency of bubble formation. Several

definitions of these terms appear in the literature (Hsu and Graham, 1961; Han and Griffith, 1965; Shoukri and Judd, 1978).

Many static models have appeared in the literature which basically have attempted to develop expressions for the wall superheats required for the bubble nucleation on a surface. The prominent ones are briefly described below.

Most of these assume a LTD within the thermal layer. For known wall superheats all these models can give a size or the size range of active nucleation sites.

1. Griffith and Wallis(1960) observed that equation (2.4) predicted the required superheat only for a uniformly superheated situation and this value was much lower than the actual wall superheat required for nucleating a bubble on a surface in HPB. Using artificial conical cavities of 51 μm diameter, under HPB, they observed that nucleation commenced at a wall superheat of 11K rather than the value of 1.6 K predicted by equation (2.4).

2. Hsu (1962) proposed the following equation to predict the size range of active sites

$$(R_c)_{max,min} = \frac{\delta_t(T_w-T_s)}{2C_a(T_w-T_b)} \left[1 \pm \left\{1 - \frac{8C_b\sigma T_s(T_w-T_b)}{\delta_t \rho_v h_{fg}(T_w-T_s)^2}\right\}^{1/2}\right] \quad (2.17)$$

where C_a and C_b are constants depending upon the bubble-surface contact angle and cavity geometry. The above relation gives

the nucleation superheat, ΔT_n, for saturated pool boiling ($T_b = T_s$) as

$$\Delta T_n = (T_w - T_s) = 2A_h / [1 - \{(2C_a R_c / \delta_t) - 1\}^2] \qquad (2.18)$$

From equation (2.17) one can deduce a stability criterion for sustained boiling to exist at a given nucleation site and it is given by

$$T_{w_{min}} = T_s + A_h + [A_h \{A_h + 2(T_s - T_b)\}]^{1/2} \qquad (2.19)$$

where

$$A_h = \frac{4\sigma T_s C_b}{\rho_v h_{fg} \delta_t} \qquad (2.20)$$

3. Han and Griffith (1965) gave the following expressions for the size range of active sites for a hemispherical nucleus sitting at the cavity mouth

$$R_{c_{max,min}} = \frac{\delta_t}{3} \frac{(T_w - T_s)}{(T_w - T_b)} \left[1 \pm \left\{1 - \frac{12\sigma T_s (T_w - T_b)}{\rho_v h_{fg} \delta_t (T_w - T_s)^2}\right\}^{1/2}\right] \qquad (2.21)$$

For $T_b = T_s$,

$$\Delta T_n = \frac{12 \sigma T_s}{\rho_v h_{fg} \delta_t \left[1 - \left(\frac{3R_c}{\delta_t} - 1\right)^2\right]} \qquad (2.22)$$

which can also be considered as the minimum wall superheat required to emit bubbles from a cavity of a given size.

4. Howell and Siegel (1967) developed a model for a hemispherical nucleus sitting at the cavity mouth. They used the concept of evaporation and condensation at the l-v interface. The superheats due to them are given by

$$\Delta T_n = \frac{(T_e - T_s)}{(1 - \frac{R_c}{2\,\delta_t})} \qquad R_c \leq \delta_t \tag{2.23}$$

$$\Delta T_n = \frac{2R_c}{\delta_t}(T_e - T_s) \qquad R_c \geq \delta_t \tag{2.24}$$

where $(T_e - T_s)$ is given by equation (2.4) with $R_i = R_c$.

5. Kant (1983) extended the nucleation model due to Howell and Siegel (1967), but neither assumed a hemispherical vapor nucleus at the cavity mouth nor a LTD. His model equations which were developed for the three TD in the thermal layer namely the LTD, NLTD and MDTD are given below.

LTD :

$$(T_w - T_b) \geq \frac{B(T_e - T_b)}{[B(1 - \frac{R_c}{\delta_t}\cot\beta) - \frac{R_c}{2\,\delta_t}]} \qquad H \leq \delta_t \tag{2.25}$$

$$(T_w - T_b) \geq \frac{2BR_c}{\delta_t}(T_e - T_b) \qquad H \geq \delta_t \tag{2.26}$$

NLTD :

$$(T_w-T_b) \geq \frac{(T_e - T_b)}{[1 - \frac{BR_c}{\delta_t} + \frac{1}{2}(\frac{BR_c}{\delta_t})^3 - \frac{1}{5}(\frac{BR_c}{\delta_t})^4]} \qquad H \leq \delta_t \qquad (2.27)$$

$$(T_w-T_b) \geq \frac{10}{3} BR_c (T_e-T_b) \qquad H \geq \delta_t \qquad (2.28)$$

MDTD :

$$(T_w-T_b) \geq \frac{BR_c(T_e - T_b)}{\delta_t[(a - \frac{a^2}{2}) + (\frac{d}{1-n}) \{[\frac{R_c}{\delta_t} B^{1-n}] - a^{1-n}\}]}$$

$$H \leq \delta_t \qquad (2.29)$$

$$(T_w-T_b) \geq \frac{BR_c(T_e - T_b)}{\delta_t[(a - \frac{a^2}{2}) + \frac{d}{1-n}(1-a^{1-n})]} \qquad H \geq \delta_t \qquad (2.30)$$

where $B = \frac{1 + \cos \beta}{\sin \beta}$ (2.31)

and β = angle which the bubble surface makes with the boiling surface (shape angle).

The predicted wall superheats for the NLTD were higher than those for the LTD and MDTD. Besides the effect of TD, his model also incorporated the effect of the shape angle, β. Three values of β namely $\beta = \pi/2$, $(\pi/2 + \theta)$ and θ were used,

where θ was the dynamic contact angle for the surface-liquid combination. The value of $\beta = \pi/2$ corresponded to the hemispherical shape of the bubble, but not the other two values. The values $\beta = \theta$ and $(\pi/2 + \theta)$ were shown to be important with reference to his dynamic bubble nucleation model (discussed in Section 2.6).

2.6 DYNAMIC BUBBLE NUCLEATION MODELS IN HPB

All static models of nucleation superheat assumed the presence of a vapor nucleus on the cavity mouth and the nucleation criterion was satisfied when the l-v interface was exposed to the bulk liquid. Such models say nothing about the mechanism of nucleation and site deactivation. The vapor nucleus grows when the thermal layer is re-established. The site is considered active if the waiting time is finite. Many dynamic models have been proposed to simulate the bubble nucleation and site deactivation mechanisms, which are briefly described below.

1. Bankoff (1959) modeled the bubble nucleation problem as viscosity controlled cavity penetration due to vapor condensation. He did not predict the reversal of the motion of l-v interface.
2. Marto and Rohsenow (1966) neglected the interface motion in their energy balance and derived a dimensionally incorrect equation to predict the interface motion.

3. Fabic (1964) used both advancing and receding contact angles, the data for which are not readily available. The superheat predicted by him is likely to be much lower than the actual wall superheat needed for nucleation.

4. Singh et al. (1976) developed a model for the stability of a nucleation site considering transient heat flux, inertial and viscous effects of the liquid. The time required for the interface penetration was taken to be zero which is not in conformity with the experiments.

5. Kant (1983) based upon his boiling nucleation experiments on single sites in the pool boiling of organic liquids and their mixtures, threw light on the Bubble Nucleation and Site Deactivation Mechanisms. Based upon his observations, he proposed a dynamic single bubble nucleation model which predicted the waiting time of a bubble for given boiling conditions. This model took into account the flow of liquid into the nucleation site and the time variation of the surface temperature through an additional model proposed for the same. Other features of his model which were not considered in the earlier models for predicting t_w, were the condensation and evaporation at the l-v interface, pressure losses during the flow and the modeling of flow within the cavity. Both

Hagen-Poiseuille and Suddenly Accelerated Flows were considered within the cavity. The predictions of the model were in agreement with the experimental observations and the data.

The above model established an implicit site stability criterion for a given cavity diameter, degree of superheat and degree of subcooling and a given surface-liquid combination. His other criterion was directly based upon his observed, site deactivation mechanism and was explicitly expressed as a limitation on the vapor volume within the site which predicted a particular value of (L/D_c) ratio for the site to be stable. The computation of this ratio made use of the model described above. The predicted ratio was in agreement with that for cavities in a natural surface. For initial penetration of the liquid, a minimum aspect ratio (L/D_c) purely as a function of Θ was suggested.

CHAPTER 3

THERMAL LAYER THICKNESS AND NUCLEATION SUPERHEATS IN POOL BOILING

3.1 INTRODUCTION

The thermal layer thickness, δ_t, as defined in Section 1.1 has been used extensively in the pool boiling literature, but no proper method exists for its determination. Most of the static models for bubble nucleation use this parameter in their expressions, but its value ultimately is computed from some empirical expressions suggested for water and a few organic liquids based upon limited and rather unreliable experimental data. These expressions model δ_t as a function of liquid thermal conductivity and heat transfer coefficient. Many authors have also talked about the upper and lower bounds of δ_t corresponding to the free convection and pool boiling situation respectively. An attempt is made here to develop a general expression for δ_t and based upon its value predict the boiling nucleation superheats and the size range of active sites.

3.2 MODELLING OF THERMAL LAYER THICKNESS

Nucleate boiling on a metallic surface is dependent upon the fluid properties, heat flux, degrees of superheat and subcooling and the surface roughness. It is postulated here that

the existing expressions for δ_t, in the literature, are too simple to be realistic for any given boiling conditions and all the aforementioned parameters should be included in developing an expression for it. This is done here using the 'Dimensional Analysis'. The degree of subcooling is not considered here.

As mentioned above, δ_t can be written as a function of fluid and vapor properties, heat flux, $\dot{q}$, degree of superheat, ΔT, cavity diameter, D_c, and surface roughness, S_R. Then,

$$\delta_t = fn\ (\dot{q},\ T_w - T_s,\ \rho_v, \rho_1,\ h_{fg},\ \sigma,\ D_c,\ \mu_1,\ k_1,\ c_1,\ S_R) \tag{3.1}$$

The dimensions of the different quantities are given in Appendix B.

Using the Buckingham's π theorem and taking $\Delta T, \rho_1, D_c, \dot{q}$ as the repeating variables, one can obtain the following eight π's or the dimensionless groups.

$$\begin{aligned}
\pi_1 &= \delta_t / D_c \\
\pi_2 &= \rho_v / \rho_1 \\
\pi_3 &= \rho_v\ h_{fg}\ D_c^2 / \dot{q} \\
\pi_4 &= \sigma\ D_c / \dot{q} \\
\pi_5 &= \mu_1 / (\rho_1 \dot{q})^{1/2} \\
\pi_6 &= k_1\ \rho_1^{1/2}\ D_c^2\ \Delta T / \dot{q}^{3/2} \\
\pi_7 &= \rho_1 c_1\ D_c^2\ \Delta T / \dot{q} \\
\pi_8 &= S_R / D_c
\end{aligned} \tag{3.2}$$

Using equation (3.2), equation (3.1) can, therefore, be written as

$$\pi_1 = fn(\pi_2, \pi_3, \pi_4, \pi_5, \pi_6, \pi_7, \pi_8) \tag{3.3}$$

Defining π_2^*, π_3^* and π_4^* as follows :

$$\pi_2^* = \pi_3\pi_7 = [\rho_1 c_1 \Delta T/ \rho_v h_{fg}] = J_a \ (\text{Jakob Number}) \tag{3.4}$$

$$\pi_3^* = \pi_4\pi_8 = \sigma S_R/\dot{q} \tag{3.5}$$

and

$$\pi_4^* = \pi_5\pi_6 = k_1 \mu_1 D_c^2 \Delta T/\dot{q}^2 \tag{3.6}$$

Using equations (3.4) through (3.6), equation (3.1) can be written as

$$\pi_1 = fn(\pi_2^*, \pi_3^*, \pi_2, \pi_4^*)$$

$$\frac{\delta_t}{D_c} = fn\left(J_a, \frac{\sigma S_R}{\dot{q}}, \frac{\rho_v}{\rho_1}, \frac{k_1 \mu_1 D_c^2 \Delta T}{\dot{q}^2}\right)$$

$$\frac{\delta_t}{D_c} = C_{sf}(J_a)^{\varepsilon_1} \left(\frac{\sigma S_R}{\dot{q}}\right)^{\varepsilon_2} \left(\frac{\rho_v}{\rho_1}\right)^{\varepsilon_3} \left(\frac{k_1 \mu_1 D_c^2 \Delta T}{\dot{q}^2}\right)^{\varepsilon_4} \tag{3.7}$$

where C_{sf} - constant depending upon surface-liquid combination.

Taking logarithms on both sides, yields

$$\varepsilon_1 \log(J_a) + \varepsilon_2 \log\left(\frac{\sigma S_R}{\dot{q}}\right) + \varepsilon_3 \log\left(\frac{\rho_v}{\rho_1}\right) + \varepsilon_4 \log\left(\frac{k_1 \mu_1 D_c^2 \Delta T}{\dot{q}^2}\right)$$

$$= \log \frac{\delta_t}{D_c C_{sf}} \tag{3.8}$$

The indices ε_1, ε_2, ε_3 and ε_4 can be obtained by solving equation (3.8) if atleast four experimental values of δ_t and corresponding values of other parameters are available for a boiling liquid.

3.3 BUBBLE NUCLEATION MODEL FOR POOL BOILING

Kant's (1983) 'Static Single Bubble Nucleation Model' for determining the wall superheat required for the incipience of bubble formation is extended here to incorporate a generalized temperature distribution, within the thermal layer, proposed here. The model takes into account the condensation and evaporation at the l-v interface. If y represents the distance measured from the surface into the body of the liquid, then at $y = 0$, $T = T_w$ and at $y = \delta_t$, $T = T_b$; $y = \delta_e$ denotes the position where $T = T_e$. Evaporation at the l-v interface will occur in the region $0 \leq H \leq \delta_e$ and condensation in the regions $\delta_e \leq H \leq \delta_t$ and $H \geq \delta_t$.

The following three cases are considered (Kant, 1983) :

Case (i) : $0 \leq H \leq \delta_e$

Fig. 3.1 shows a vapor nucleus of height, H, on a surface at temperature T_w. Using polar coordinates (r, ϕ, Ψ), and assuming axial symmetry, the heat transfer to the bubble nucleus of radius R_b by evaporation can be written as

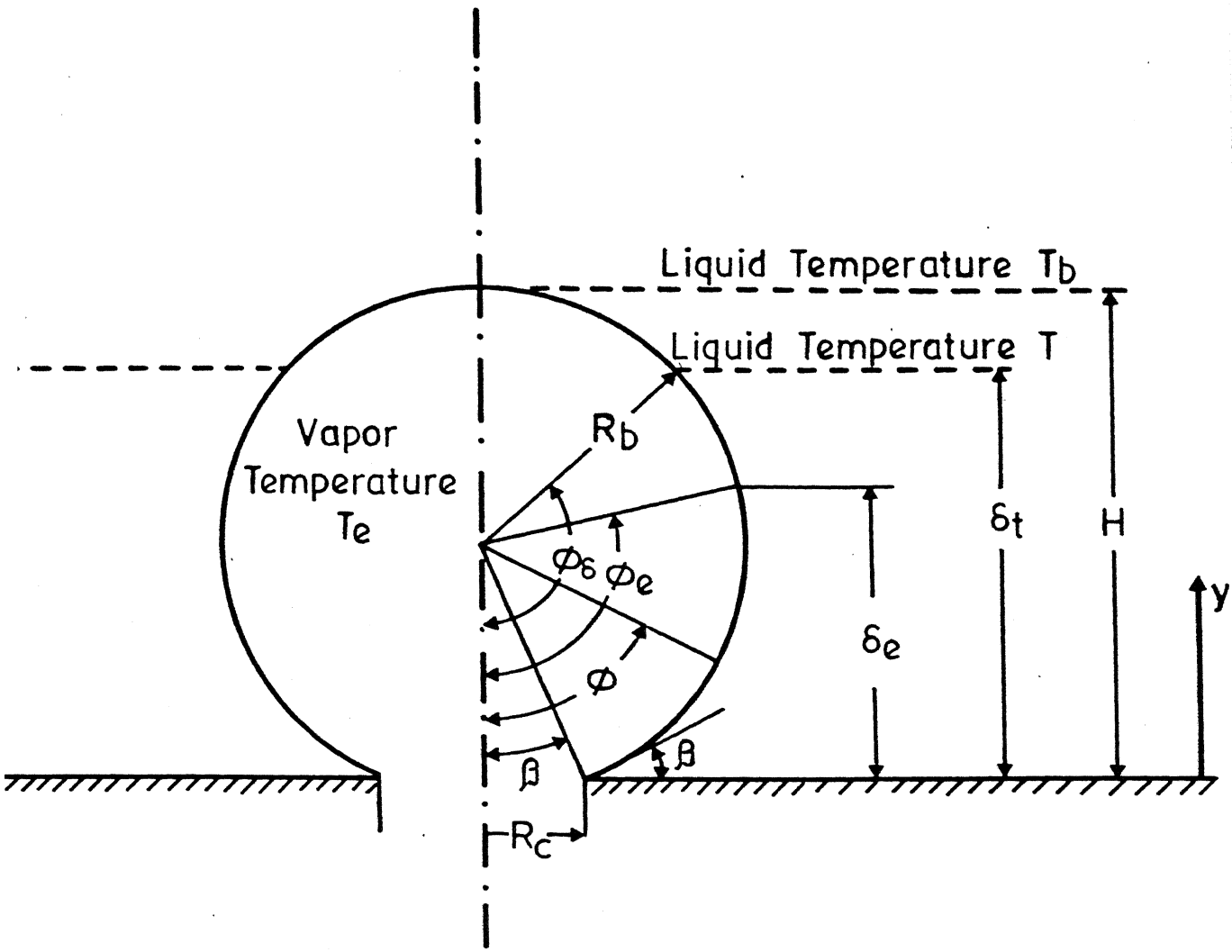

Fig. 3.1 Vapor nucleus at a cavity of radius R_c .

$$Q_1 = 2\pi h R_b^2 \int_{\beta}^{\pi} (T-T_e) \sin \phi \, d\phi \qquad (3.9)$$

where

β = the angle which the bubble surface makes with the boiling surface

T = liquid temperature within the thermal layer

T_e = equilibrium vapor temperature

Case (ii) : $\delta_e \leq H \leq \delta_t$

Considering both evaporation and condensation at the l-v interface, the net heat transfer over the bubble surface, in this case as well, is given by equation (3.9).

Case (iii) : $H \geq \delta_t$

Again taking into consideration the evaporation and condensation at the l-v interface, the net heat transfer over the bubble surface is given by

$$Q_2 = 2\pi h R_b^2 \left[\int_{\beta}^{\phi_\delta} (T-T_e) \sin \phi \, d\phi - (T_e-T_b)(1+\cos \phi_\delta) \right] \qquad (3.10)$$

In both equations (3.9) and (3.10) R_b can be replaced, for a spherical bubble, by

$$R_b = R_c / \sin \beta \qquad (3.11)$$

Height, H, of the bubble nucleus is given by

$$H = R_c \left(\frac{1 + \cos \beta}{\sin \beta} \right) \qquad (3.12)$$

From Fig. 3.1, ϕ_δ corresponding to $y = \delta_t$ can be expressed as

$$\cos \phi_\delta = \cos \beta - (\delta_t \sin \beta / R_c) \tag{3.13}$$

For the three cases mentioned above, the net heat transfer rates Q_1 and Q_2 can be determined if the temperature distribution within the thermal layer is known.

Let the temperature distribution within the thermal layer be expressed as a polynomial

$$\xi = a_o + a_1\eta + a_2\eta^2 + a_3\eta^3 + a_4\eta^4 \tag{3.14a}$$

where

$$\xi = \frac{T-T_b}{T_w-T_b} \quad \text{and} \quad \eta = \frac{y}{\delta_t} \tag{3.14b}$$

From Fig. 3.1

$$y = R_b(\cos \beta - \cos \phi) \tag{3.15}$$

Substituting equation (3.14) into equations (3.9) and (3.10), using equation (3.15) and replacing $(1+\cos \beta)/\sin \beta$ by B yields

$$Q_1 = \frac{2\pi h R_c^2}{\sin \beta} \times B \times (T_w-T_b) \left[a_o + \frac{a_1 R_c B}{2 \delta_t} + \frac{a_2 R_c^2 B^2}{3 \delta_t^2} + \frac{a_3 R_c^3 B^3}{4 \delta_t^3} + \frac{a_4 R_c^4 B^4}{5 \delta_t^4}\right] - \frac{2\pi h R_c^2 B (T_e-T_b)}{\sin \beta} \tag{3.16}$$

$$Q_2 = \frac{2\pi h R_c^2}{\sin^2\beta}\left[(T_w-T_b)\,\delta_t\,\frac{\sin\beta}{R_c}\left\{a_o + \frac{a_1}{2} + \frac{a_2}{3} + \frac{a_3}{4} + \frac{a_4}{5}\right\}\right.$$

$$\left. - (T_e-T_b)(1+\cos\beta)\right] \qquad (3.17)$$

For the nucleus to grow both $Q_1 \geq 0$ and $Q_2 \geq 0$ yields (see equations (3.16) and (3.17))

$$(T_w-T_b) \geq \frac{(T_e-T_b)}{\left[a_o + \frac{a_1 R_c B}{2\,\delta_t} + \frac{a_2 R_c^2 B^2}{3\,\delta_t^2} + \frac{a_3 R_c^3 B^3}{4\,\delta_t^3} + \frac{a_4 R_c^4 B^4}{5\,\delta_t^4}\right]} \qquad (3.18)$$

$$(T_w-T_b) \geq \frac{R_c B(T_e - T_b)}{\delta_t\left[a_o + \frac{a_1}{2} + \frac{a_2}{3} + \frac{a_3}{4} + \frac{a_4}{5}\right]} \qquad (3.19)$$

Equations for a hemispherical nucleus can be obtained from equations (3.18) and (3.19) by substituting $B = 1$ corresponding to $\beta = \pi/2$.

3.4 SIZE RANGE OF ACTIVE SITES

The equations developed in the preceding section yield wall superheat required for bubble nucleation as a function of (T_e-T_b), R_c and δ_t. For a given R_c, (T_e-T_b) can be calculated from equation (2.4) and δ_t can be computed from equation (3.8). If nucleate boiling superheat is known for a surface, then the size range of active sites in it can be determined from equations (3.18) or (3.19).

3.5 PREDICTIONS

Based upon the equations developed in the preceding sections, computations were made for the thermal layer thickness, nucleation superheats and the size range of active sites which are discussed below.

3.5.1 Thermal Layer Thickness (δ_t)

In order to determine δ_t, the indices in equation (3.7) were determined using the available values of δ_t for pentane. These indices are given in Table 3.1.

Table 3.1

ε's for Pentane

ε_1	ε_2	ε_3	ε_4
1.5	1.9	-1.3	-0.5

Using these indices, δ_t was computed for Pentane from equation (3.7) for given values of ΔT and $\dot{q}$, which were found to be in good agreement with the reported values as shown in Figures 3.2 and 3.3 for pentane and water respectively. The values of δ_t due to Lippert and Dougall (1968) were computed

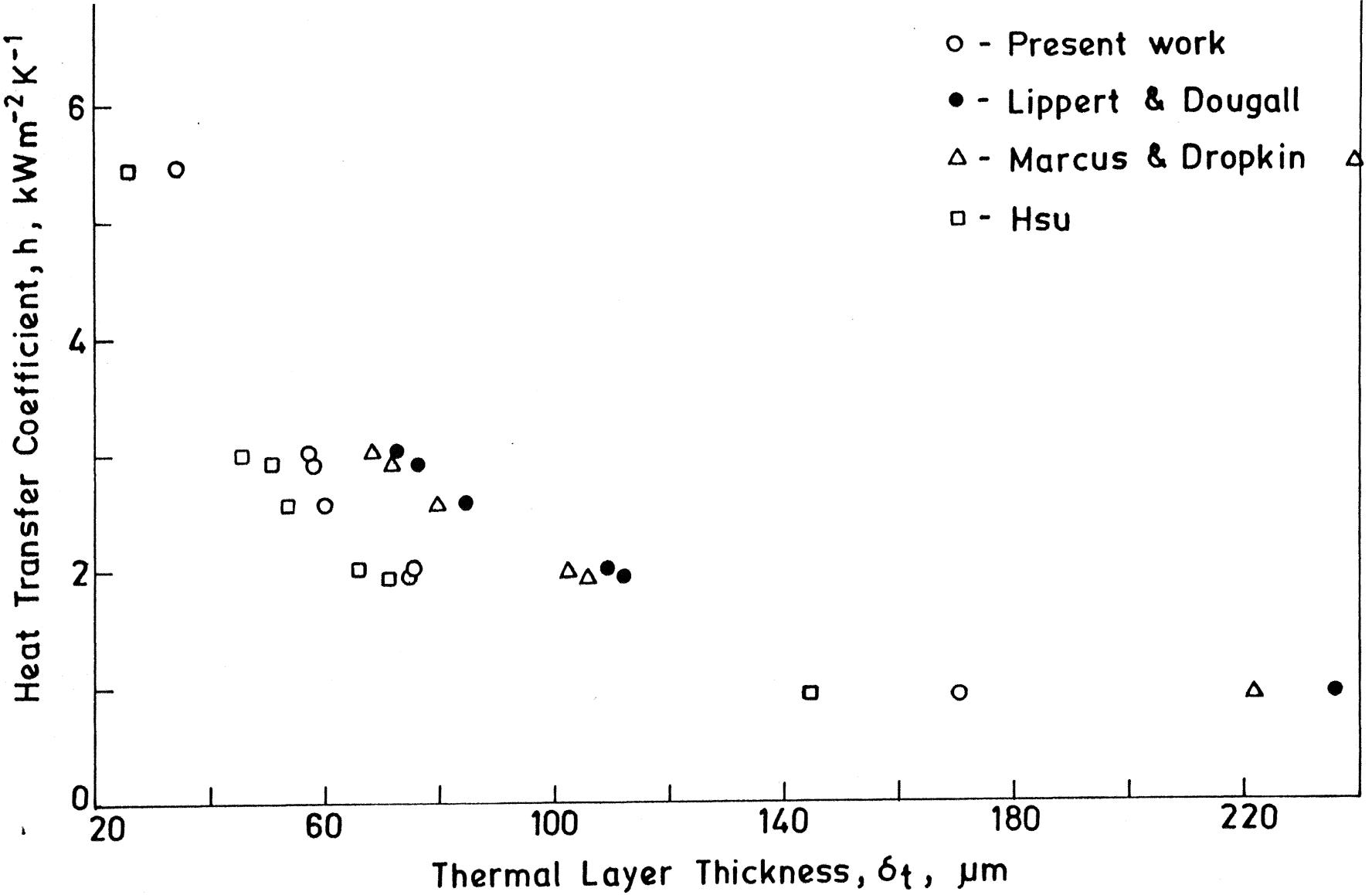

Fig. 3.2 Variation of thermal layer thickness with heat transfer coefficient for pentane.

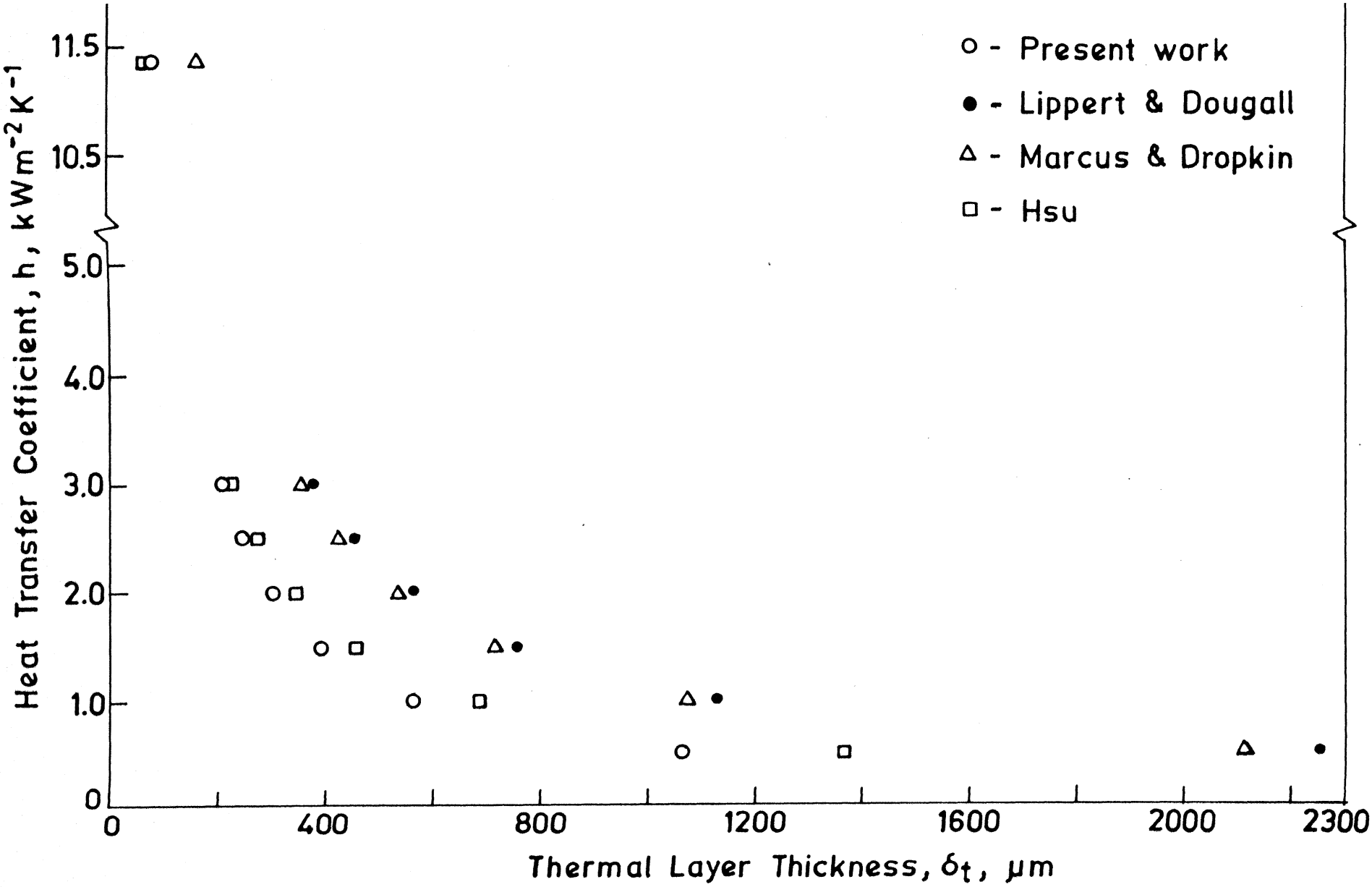

Fig. 3.3 Variation of thermal layer thickness with heat transfer coefficient for water.

from $\delta_t = 1.65\ k_1/h$, whereas those due to Marcus and Dropkin (1965) were computed from $\delta_t = 1.57\ k_1/h$ for $h \leq 3970$ W $m^{-2}K^{-1}$ and $\delta_t = 0.0177\ h^{-0.5}$ for $h \geq 3970$ W $m^{-2}K^{-1}$. Hsu (1962) used the data of Clark, Westwater and Strenge (1959) and modeled it simply as $\delta_t = k_1/h$. The values of δ_t computed from equation (3.7) are also shown in the figure. It can be seen from it that the predicted values of δ_t are in good agreement with the values of Hsu (1962) with the values of Hsu (1962), which led to the conclusion that the simpler modeling $\delta_t = k_1/h$ was just as good as the modeling presented by equation (3.7). The parameters $\dot{q}$, ΔT and k_1 seem to have more pronounced effect on δ_t than any other variable. But as the available data on δ_t is rather unreliable, the author strongly feels that this comparison is inconclusive. The real comparison can be made only when realistic data on δ_t become available. It may be noted that if the values of Lippert and Dougall (1968) and those of Marcus and Dropkin (1965) are divided respectively by 1.65 and 1.57, the resulting values will be found in good agreement with the values of Hsu (1962) and those presented here except the first value for Pentane and the last for water which were calculated using $\delta_t = 0.0177\ h^{-0.5}$.

3.5.2 Temperature Distribution in the Thermal Layer

Three TD's namely LTD, NLTD and MDTD for the thermal layer were discussed earlier. Only for the NLTD, predicted values of

ΔT_n were higher than those for other TD's (Kant, 1983).

The reported experimental values for bubble nucleation on a surface are still higher than the predicted values. Hence it was attempted to propose a TD in the thermal layer which would bring a closer agreement with the experimental data. The proposed TD is given by equation (3.14a) and the constants are given in Table 3.2.

Table 3.2

Constants in the Temperature Distribution

a_o	a_1	a_2	a_3	a_4
1.0	-2.8	1.0	2.0	-1.0

3.5.3 Bubble Nucleation Superheats (ΔT_n)

The model presented in Section 3.3 related ΔT_n to D_c, δ_t, (T_e-T_s) and the constants of the T D in the thermal layer. For a given liquid boiling on a surface having a cavity of diameter, D_c, ΔT_n could be computed if δ_t was known. In the results presented below,

δ_t was computed for different values of h (i.e., different values of $\dot{q}$ and (T_w-T_s)). These values of δ_t were then used

to compute ΔT_n for given D_c and shape angle, β.

The effect of increasing δ_t, keeping other factors unchanged, was a decrease in the value of ΔT_n. As mentioned earlier, three values of β, namely, $\beta = \Theta$, $\pi/2$ and $\pi/2 + \Theta$ were used to calculate ΔT_n. These are plotted in Fig. 3.4 showing the variation of ΔT_n with δ_t for aforementioned values of β. It can be clearly seen from these curves that predicted ΔT_n are higher from $\beta = \Theta$ than those for $\beta = \pi/2$ and $\pi/2 + \Theta$. The author strongly feels that as $\beta = \Theta$ is a characteristic of a surface liquid combination while other values are not, the former should be considered for calculating ΔT_n. Shape angle, β, as defined earlier will keep on changing continuously right from the moment a l-v interface can be seen on the heated surface to the moment of bubble departure. For these reasons, the assumption of other authors of a hemispherical vapor nucleus sitting on a cavity mouth, is unreasonable.

The values of ΔT_n were also computed for various values of D_c, keeping δ_t unchanged. The constants a_i ($i = 0,1, \ldots, 4$) of the TD given in table were used. The trend of the predictions as shown in Fig. 3.5 is similar to those of Howell and Siegel (1967) and Kant (1983), but the predicted values of ΔT_n are somewhat higher than those of other authors.

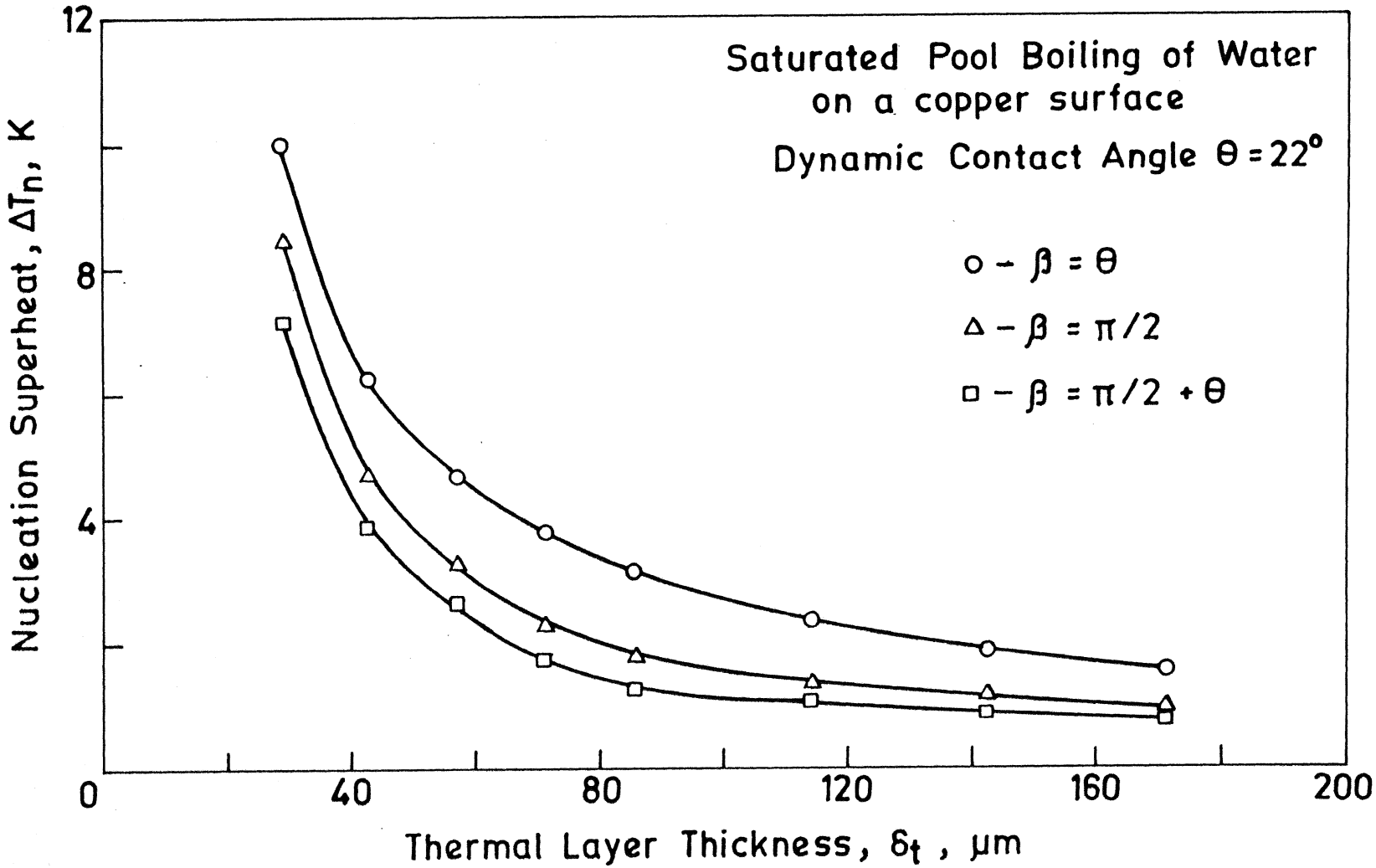

Fig. 3.4 Variation of nucleation superheat with thermal layer thickness for water.

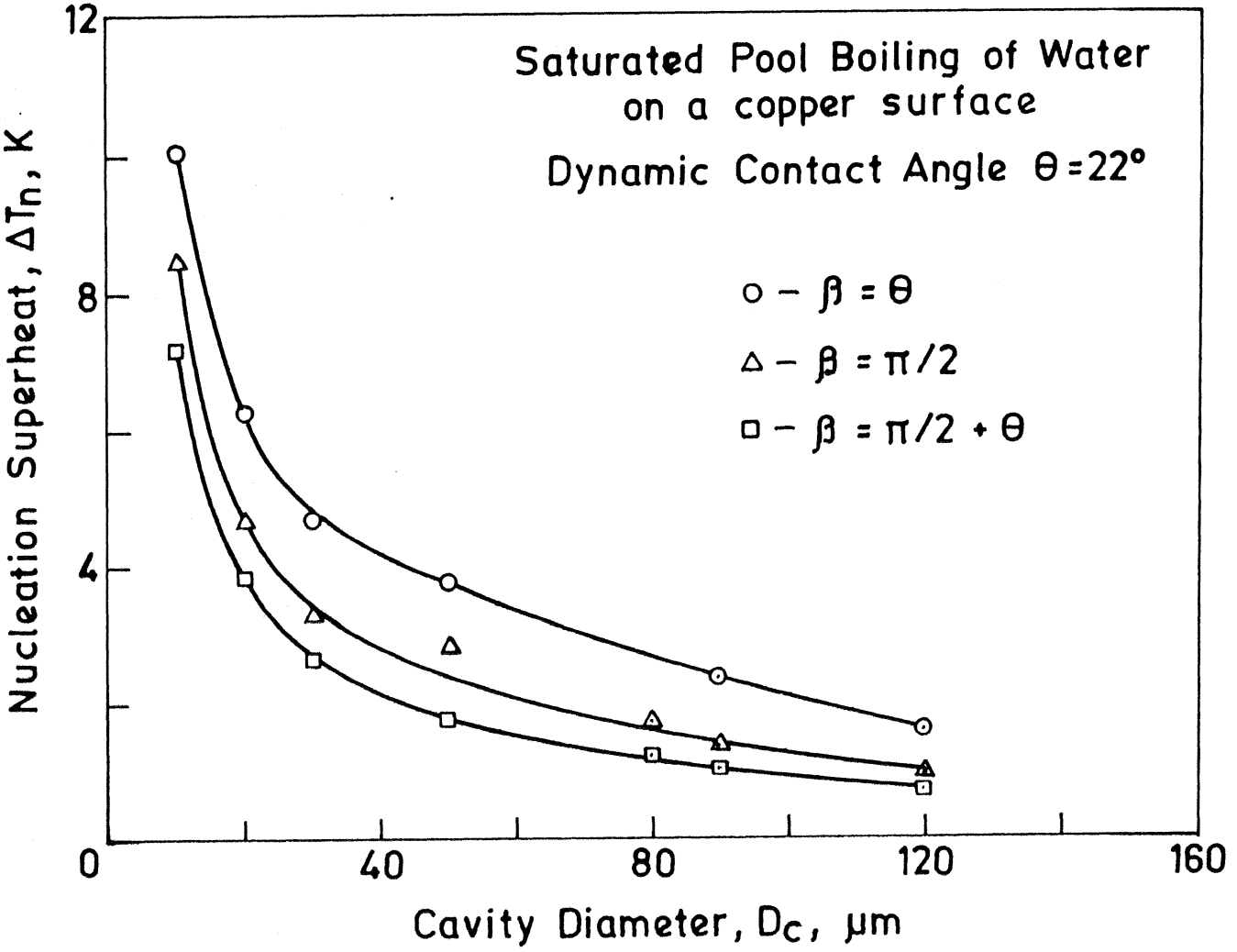

Fig. 3.5 Variation of nucleation superheat with cavity diameter for water.

3.5.4 Size Range of Active Sites

The equations (3.18) and (3.19) in the preceding section related (T_w-T_s) to (T_e-T_b), R_c and θ. For a given boiling liquid, R_c and θ, it is easy enough to compute the minimum degree of superheat required to nucleate a bubble from the surface. As can be seen from Fig. 3.5, as the cavity size increases, required minimum degree of superheat decreases. This evidently means that a given degree of superheat should activate a particular size of the cavity and theoretically speaking all other larger cavities existing in the surface. This refers to a particular size range of cavities that must be activated for a given degree of superheat. Pool boiling experiments reveal that the cavities which are actually activated probably because of their inability to entrap vapor.

Equation (3.18) can be solved for R_c for given values of (T_w-T_s), δ_t, θ and boiling liquid properties. This solution will give only two positive real roots which will comprise the size range of active sites. The size range computed using the proposed TD in the nucleation model is given in Table 3.3, along with those due to Hsu (1962) and Han and Griffith (1965). The cavities near the lower end of the size range nucleate while those near the upper end do not. Although the predicted range covers a wider spectrum of cavities, it is still pretty hard to say whether or not these large cavities will nucleate

Table 3.3 Comparison of size range of active sites boiling liquid water

T	δ_t	Present work		Han and Griffith		Hsu	
K	μm	R_c min μm	R_c max μm	R_c min μm	R_c max μm	R_c min μm	R_c max μm
4.0	15.0	2.92	34.18	3.19	6.81	2.64	12
	20.0	2.64	45.78	2.74	10.59	2.48	17
	25.0	2.51	57.38	2.57	14.41	2.41	22
5.0	15.0	2.15	34.31	2.24	7.76	2.01	12
	20.0	2.02	45.90	2.06	11.28	1.92	18
	25.0	1.95	57.49	1.97	14.69	1.88	23

or serve as stable nucleation sites. Although the experimental evidence of the activity of smaller sites is available, yet the same questions could be raised about them. Possible explanations might be that the smaller cavities may entrap vapor more easily and may generally have the geometry (L/D_c ratio etc.), to act as stable sites. In this context, nucleation of cavities in the upper size range may be decided by other factors as well and not the degree of superheat and thermal layer thickness alone.

Solution of equation (3.19) for given R_c, (T_w-T_b), δ_t and θ, results in a single cavity size which must nucleate. Any cavities larger than this will nucleate if other requirements (geometry etc.) are satisfied. It may be noted here that this equation can be used only for subcooled pool boiling.

CHAPTER 4

DYNAMIC MODEL FOR BOILING NUCLEATION STABILITY

4.1 INTRODUCTION

During boiling, vapor bubbles nucleate and grow from prescribed sites in the surface, called as active sites. Those sites which cannot trap vapor within them are called inactive sites. The steps in the life cycle of a bubble are shown in Fig. 4.1 which are based upon the experimental observations of Kant (1983) on single nucleation sites. His photographic data showed the movement of liquid-vapor interface within the cavity and the presence of some liquid at the bottom of the cavity.

As soon as a fully grown bubble lifts off from a cavity, the cold liquid partly from the thermal layer and the rest from the bulk rushes into the cavity and penetrates upto a certain depth. The temperature of this liquid, T_o, may be such that $T_b \leq T_o \leq T_w$. The initial penetration is assumed to take place in a negligibly small amount of time. At the same time it is assumed that a very small amount of liquid left at the bottom of the cavity, at the vapor temperature when a bubble departs, cools down almost to the saturation temperature of the liquid due to flow of bulk liquid into the cavity at the moment of departure. Thus an elongated vapor bubble is entrapped

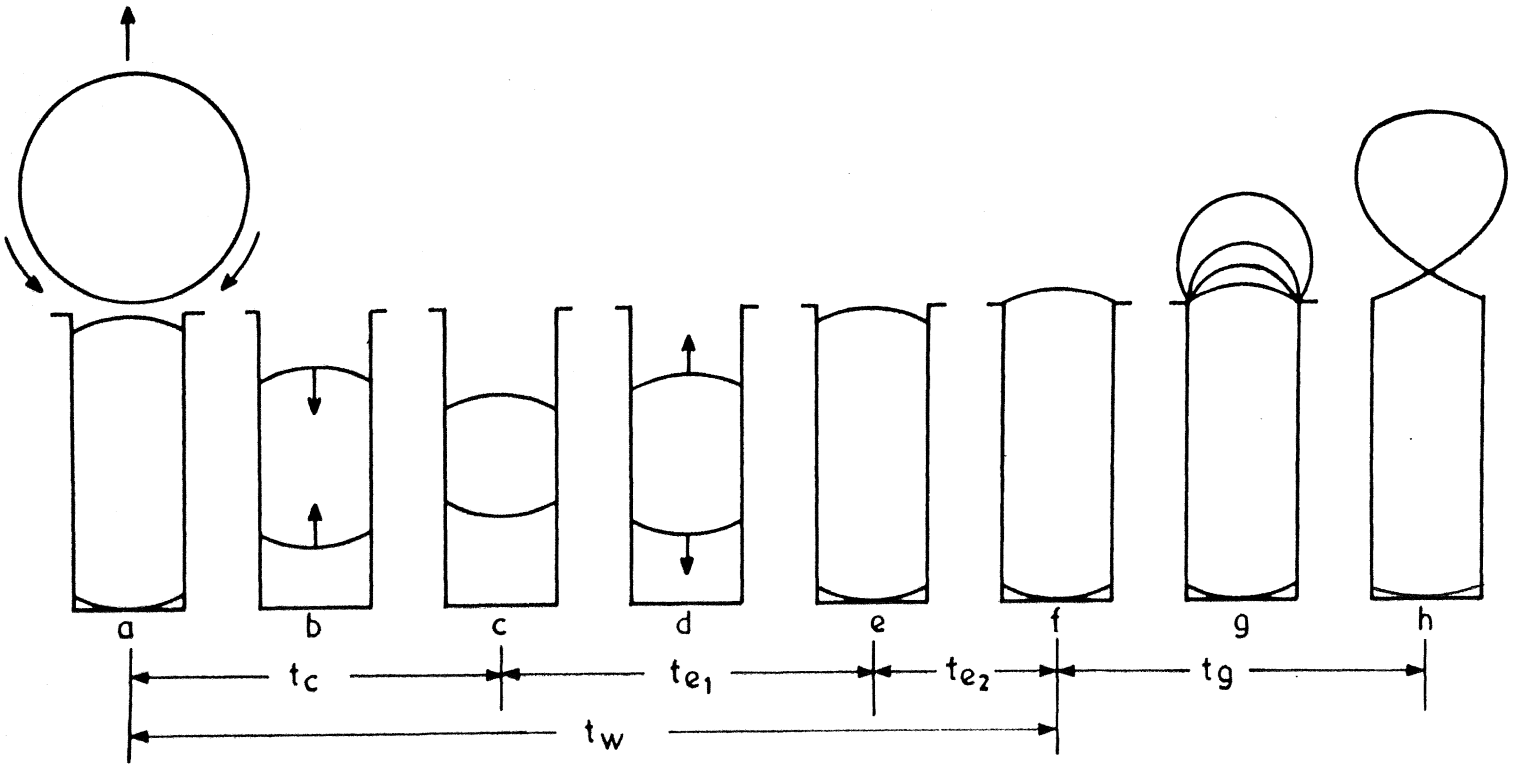

Fig. 4.1 Diagram of proposed nucleation cycle showing the upper and lower l-v interface positions.

inside the cavity between the liquid at the top and that at the bottom. Owing to the curvature of the l-v interfaces, the vapor trapped inside the cavity is at a higher pressure than that of the liquid. Since the temperature of the liquid in the Upper Liquid Control Volume (ULCV), T_o, and that in the Lower Liquid Control Volume (LLCV), T_s, are less than the saturation temperature of this vapor, condensation begins to occur. The upper l-v interface recedes into the cavity and the lower l-v interface rises up inside the cavity as the condensation continues. At the same time, since the surface temperature, which has to be higher than the vapor temperature for the boiling to occur on a metallic surface, conducts heat from the cavity walls into the ULCV and the LLCV, which increases the liquid temperatures. At the same time the condensation heat transfer across the two l-v interfaces, further increases the liquid temperature inside the control volumes. The condensation phase ends when the temperature in both the control volumes reach the vapor temperature, T_v. The time elapsed during this phase is the condensation time, t_c. The wall temperature during the process is assumed to be at a constant value, T_w.

Once the liquid temperatures have reached the vapor temperature, any additional heat transfer from the cavity walls goes to evaporate the liquid at the l-v interfaces. This

introduces the evaporation phase which has been split into two phases, namely, first evaporation phase and second evaporation phase.

During the first evaporation phase, the heat supplied from the cavity walls to the liquid in the ULCV and LLCV starts the evaporation of the liquids at the two interfaces. During the evaporation, the upper l-v interface starts to rise toward the cavity mouth and the lower l-v interface starts receding towards the bottom of the cavity. The first evaporation comes to an end when the upper l-v interface just flushes the surface. By this time, it is assumed that the lower l-v interface is at its lowermost position. The time elapsed during this phase is, t_{e_1}, as shown in Fig. 4.1.

During the second evaporation phase the upper l-v interface just protrudes out of the cavity and appears as a nucleus at the mouth of the cavity. During this period, the lower l-v interface remains at the bottom of the cavity. The time elapsed during this phase is t_{e_2}.

The sum $(t_{e_1}+t_{e_2})$ is the total evaporation time. The sum of the condensation and evaporation times (t_c+t_e) is the waiting period, t_w, for a nucleating bubble. This bubble nucleus grows at the site to its maximum diameter during the growth period, t_g. The sum (t_w+t_g) is the period of the bubble cycle which repeats itself.

If the liquid temperature never reaches the vapor temperature, all the vapor will continue to condense, leading to a complete collapse of the cavity.

The various steps shown in Fig. 4.1 are :

a. Departure of the fully grown bubble from the surface and initial penetration of the liquid into the cavity.

b. Condensation at the liquid-vapor interfaces.

c. End of condensation.

d. Evaporation at the liquid-vapor interfaces.

e. End of first evaporation phase.

f. End of second evaporation phase.

g. Growth of the bubble at the cavity mouth to its maximum diameter.

Based upon the above considerations, the dynamic model of Kant (1983) and Kant and Weber (1986a, 1986b, 1986c) for the nucleation of a bubble in HPB of a liquid is extended here to predict the waiting time, t_w.

4.2 ASSUMPTIONS MADE IN THE MODEL

The nucleation cavity is cylindrical in shape.

The l-v interfaces retain their spherical shape during motion inside the cavity.

The pressure just outside the cavity, p_{1_o}, is equal to the system pressure.

4. At zero time, there is an initial penetration of the liquid into the cavity and a small amount of liquid is present at the bottom of the cavity at the saturation temperature, T_s.
5. The pressure and density of the trapped vapor within the cavity remain constant during the nucleation process.
6. The vapor temperature, T_v, remains constant during the bubble nucleation.
7. The temperature of the surface and that of the cavity walls, T_w, is a constant.
8. There are no thermal gradients existing within the vapor inside the cavity and hence the temperature of the interface is the same as the temperature of the vapor.

4.3 CONDENSATION PHASE

The initial penetration is assumed to take place in a negligibly small time. Condensation starts immediately at the l-v interfaces.

4.3.1 Mass Balances

During the condensation phase, as the upper l-v interface (ULVI) moves into the cavity some liquid from the bulk flows into it. The lower l-v interface (LLVI) rises up inside the cavity as the condensation proceeds and some vapor is condensed at the interfaces. Let $\dot{m}_{l_1}$, $\dot{m}_{c_1}$ and $\dot{m}_{c_2}$ represent the mass flow

rate of liquid flowing into the cavity and the rates of condensation of vapor at the upper and lower interfaces respectively. Let M_{1_1}, M_{1_2} and M_v represent the mass of liquids and vapor respectively at any time t within the ULCV, LLCV and vapor control volume (VCV) shown in Fig. 4.2.

The mass balances over the liquid and vapor control volumes yield,

$$\dot{m}_{1_1} + \dot{m}_{c_1} = \frac{dM_{1_1}}{dt} \tag{4.1}$$

$$-(\dot{m}_{c_1} + \dot{m}_{c_2}) = \frac{dM_v}{dt} \tag{4.2}$$

$$\dot{m}_{c_2} = \frac{dM_{1_2}}{dt} \tag{4.3}$$

M_{1_1}, M_{1_2} and M_v are given by

$$M_{1_1} = [\frac{\pi D_c^2}{4} z_1 - V_{sc}] \rho_1 \tag{4.4}$$

$$M_{1_2} = [\frac{\pi D_c^2}{4} (L-z_2) - V_{sc}] \rho_1 \tag{4.5}$$

$$M_v = [\frac{\pi D_c^2}{4} (z_2-z_1) + 2V_{sc}] \rho_v \tag{4.6}$$

where, V_{sc}, the volume of the spherical cap is given by (Perry and Chilton, 1973)

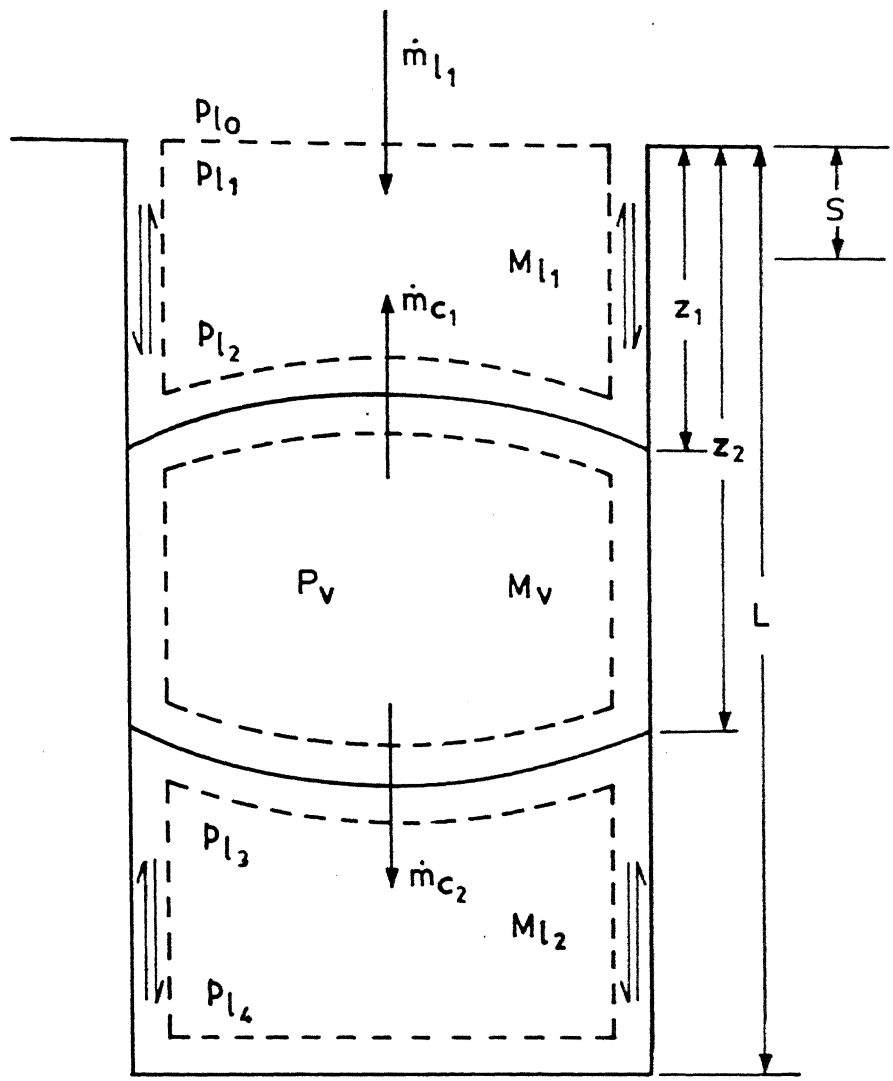

Fig. 4.2 Liquid and vapor control volumes within a cavity during the condensation phase.

$$V_{sc} = \frac{\pi D_c^3}{24\cos^3\theta} (1-\sin\theta)^2 (2+\sin\theta) \qquad (4.7)$$

During the movement of the two l-v interfaces within the cavity, the contact angle hysteresis may be disregarded and hence V_{sc} may be assumed to be constant. The densities, ρ_v and ρ_1, of vapor and liquid, respectively, are taken to be constant at the boiling point of the liquid.

Adding equations (4.1), (4.2) and (4.3) and using equations (4.4), (4.5) and (4.6), yields

$$\dot{m}_{1_1} = \frac{\pi D_c^2}{4} (\rho_1 - \rho_v) \left[\frac{dz_1}{dt} - \frac{dz_2}{dt}\right] \qquad (4.8)$$

Adding equations (4.1) and (4.2) and using equations (4.4) and (4.6) yields

$$\dot{m}_{1_1} - \dot{m}_{c_2} = \frac{\pi D_c^2}{4} \left[\rho_1 \frac{dz_1}{dt} + \rho_v\left(\frac{dz_2}{dt} - \frac{dz_1}{dt}\right)\right] \qquad (4.9)$$

The condensation heat transfer across the LLVI is given by

$$q_{ic_2} = h_{ic} A_i (T_v - T_{1_2}) \qquad (4.10)$$

where h_{ic} = film heat transfer coefficient for condensation

A_i = interfacial area given by

$$A_i = \frac{\pi D_c^2}{2(1+\sin\theta)} \qquad (4.11)$$

If h_{fg} is the enthalpy of vaporization of the liquid, the mass flow rate of the condensate, $\dot{m}_{c_2}$, into the LLCV is given by

$$\dot{m}_{c_2} = \frac{q_{ic_2}}{h_{fg}} = \frac{\pi D_c^2 \, h_{ic}(T_v - T_{1_2})}{2(1+\sin\theta)\, h_{fg}} \qquad (4.12)$$

Let V_1 be the average flow velocity inside the cavity in the ULCV, the mass flow rate, $\dot{m}_{1_1}$ can also be written as

$$\dot{m}_{1_1} = \frac{\pi D_c^2}{4} \rho_1 \, V_1 \qquad (4.13)$$

Substituting for $\dot{m}_{c_2}$ and $\dot{m}_{1_1}$, from equations (4.12) and (4.13), into equation (4.9) yields,

$$\frac{dz_1}{dt} = \frac{1}{(\rho_1 - \rho_v)} \left[\rho_1 \, V_1 - \frac{2h_{ic}(T_v - T_{1_2})}{(1+\sin\theta)\, h_{fg}} - \rho_v \frac{dz_2}{dt} \right] \qquad (4.14)$$

Again from equations (4.2) and (4.3), we get

$$-\dot{m}_{c_1} = \frac{dM_v}{dt} + \frac{dM_{1_2}}{dt} \qquad (4.15)$$

considering the condensation heat transfer across the ULVI, the mass flow rate of the condensate can be written as :

$$\dot{m}_{c_1} = \frac{q_{ic_1}}{h_{fg}} = \frac{\pi D_c^2 h_{ic}(T_v - T_{1_1})}{2(1+\sin\theta)\, h_{fg}} \qquad (4.16)$$

Substituting for M_{1_2}, M_v and $\dot{m}_{c_1}$ from equations (4.5), (4.6) and (4.16) into equation (4.15) yields,

$$\frac{dz_2}{dt} = \frac{1}{(\rho_1 - \rho_v)} \left[\frac{2h_{ic}(T_v - T_{1_1})}{(1+\sin\theta)\, h_{fg}} - \rho_v \frac{dz_1}{dt} \right] \qquad (4.17)$$

4.3.2 Momentum Balances

The momentum balance over the ULCV shown in Fig. 4.2 yields

$$(p_{1_1} - p_{1_2}) \frac{\pi D_c^2}{4} + \left(\frac{\pi D_c^2}{4} z_1 - V_{sc}\right) \rho_1 g$$

$$+ \left(\frac{\pi D_c^2}{4} \frac{dz_1}{dt} z_1\right) V_1 - \pi D_c z_1 \tau_w$$

$$= \frac{d}{dt} \left[\frac{\pi D_c^2 z_1}{4} - V_{sc}\right] \rho_1 V_1 \qquad (4.18)$$

or

$$\frac{dV_1}{dt} = g + \frac{1}{\left[z_1 - \frac{4V_{sc}}{\pi D_c^2}\right]\rho_1} \left[(p_{1_1} - p_{1_2}) - \frac{4z_1 \tau_w}{D_c}\right] \qquad (4.19)$$

where

p_{1_1} = liquid pressure just within the mouth of the cavity

p_{1_2} = liquid pressure just above the ULVI

τ_w = wall shear stress exerted by the wall on to the liquid within the ULCV .

a. Pressure loss due to sudden contraction

There is a pressure or head loss due to sudden contraction involved when the liquid flows into the cavity from outside. It is given by

$$h_{1c} = C_c \frac{V^2}{2g} \text{ meter of fluid} \tag{4.20}$$

where C_c is the coefficient of contraction which can be taken to be approximately 0.5. This head loss can be expressed in terms of a pressure loss as follows :

$$h_{1c} = C_1 V^2 \tag{4.21}$$

$$\text{where } C_1 = 1.333224 \times 10^5 \left(\frac{C_c}{2g}\right)\left(\frac{\rho_1}{\rho_{Hg}}\right) \tag{4.22}$$

ρ_{Hg} = density of mercury at room temperature.

Therefore, the pressure p_{1_1} can be written as

$$p_{1_1} = p_{1_o} - C_1 V_1^2 \tag{4.23}$$

b. Determination of p_{1_2}

The pressure, p_{1_2}, can be related to p_v by the Laplace equation :

$$p_v - p_{1_2} = \frac{2\sigma}{R_i} \tag{4.24}$$

where σ is the surface tension of the liquid at the boiling point and R_i the radius of curvature of the spherical interface which is given by $R_i \cos\theta = R_c$. The pressure, P_{1_2}, can then be written as :

$$p_{1_2} = p_v - \frac{4\sigma \cos\theta}{D_c} \tag{4.25}$$

Substituting the values of p_{1_1} and p_{1_2} from equations (4.23) and (4.25) into equation (4.19).

$$\frac{dV_1}{dt} = g + \frac{1}{[z_1 - \frac{4V_{sc}}{\pi D_c^2}]\rho_l}\left[(p_{1_o} - p_v - C_1 V_1^2 + \frac{4\sigma \cos\theta}{D_c}) - \frac{4z_1 \tau_w}{D_c}\right] \tag{4.26}$$

c. Determination of wall shear stress

The velocity distribution inside the cavity is taken to be parabolic as in the case of Hagen-Poiseuille flow. The velocity v_z in the z-direction at any radius r is given by

$$v_z = 2V_1\left[1 - \left(\frac{r}{R_c}\right)^2\right] \tag{4.27}$$

From Newton's law of viscosity

$$\tau_w = -\mu\left(\frac{dv_z}{dr}\right)_{r=R_c}$$

$$\tau_w = \frac{8V_1\mu}{D_c} \tag{4.28}$$

Substituting into equation (4.26), we get

$$\frac{dV_1}{dt} = g + \frac{1}{\left[z_1 - \frac{4V_{sc}}{\pi D_c^2}\right] \rho_1} \left[(p_{1_o} - p_v - C_1 V_1^2 + \frac{4\sigma \cos\theta}{D_c}) - \frac{32 V_1 \mu z_1}{D_c^2}\right] \quad (4.29)$$

Consider now the LLCV. Unlike the ULCV, there is no liquid inflow into it. The l-v interface will tend to rise up in the LLCV with a velocity of V_2 (-ve velocity), only due to the condensation at the LLVI. It is assumed here that the wall shear stress exerted by the wall onto the liquid acts only due to the movement of the l-v interface. The momentum balance over the LLCV yields

$$-(p_{1_4} - p_{1_3}) \frac{\pi D_c^2}{4} + \left[\frac{\pi D_c^2}{4}(L-z_2) - V_{sc}\right] \rho_1 g + \pi D_c \tau_w (L-z_2) = \frac{d}{dt}\left[\frac{\pi D_c^2}{4}(L-z_2) - V_{sc}\right] \rho_1 V_2 \quad (4.30)$$

or

$$\frac{dV_2}{dt} = g - \frac{1}{\left[(L-z_2) - \frac{4V_{sc}}{\pi D_c^2}\right] \rho_1} \left[(p_{1_4} - p_{1_3}) - \frac{4(L-z_2)\tau_w}{D_c} - \rho_1 V_2 \frac{dz_2}{dt}\right] \quad (4.31)$$

The wall shear stress τ_w is given by

$$\tau_w = -\frac{8 V_2 \mu}{D_c} \quad (4.32)$$

Substituting equation (4.32) into equation (4.31) one obtains

$$\frac{dV_2}{dt} = g - \frac{1}{[(L-z_2) - \frac{4V_{sc}}{\pi D_c^2}]} [(p_{1_4} - p_{1_3}) + \frac{32V_2\mu(L-z_2)}{D_c^2} - \rho_1 V_2 \frac{dz_2}{dt}] \quad (4.33)$$

Determination of p_{1_3} and p_{1_4}

The pressure, p_{1_3}, is assumed equal to p_{1_2}, obtained from equation (4.25).

The pressure, p_{1_4}, is given by

$$p_{1_4} = p_{1_1} + [z_1 + (L-z_2)] \rho_1 g \quad (4.34)$$

4.3.3 Energy Balance

Considering the ULCV shown in Fig. 4.3.

Sensible heat of the liquid flowing into the cavity

$$= \dot{m}_{1_1} c_1 (T_o - T_b) \quad (4.35)$$

Sensible heat of the condensate going into the ULCV

$$= \dot{m}_{c_1} c_1 (T_{1_1} - T_b) \quad (4.36)$$

Heat transfer from the vapor to the ULCV through the interface (ULVI)

$$= A_i \; h'_{i_c} \; (T_v - T_{1_1}) \quad (4.37)$$

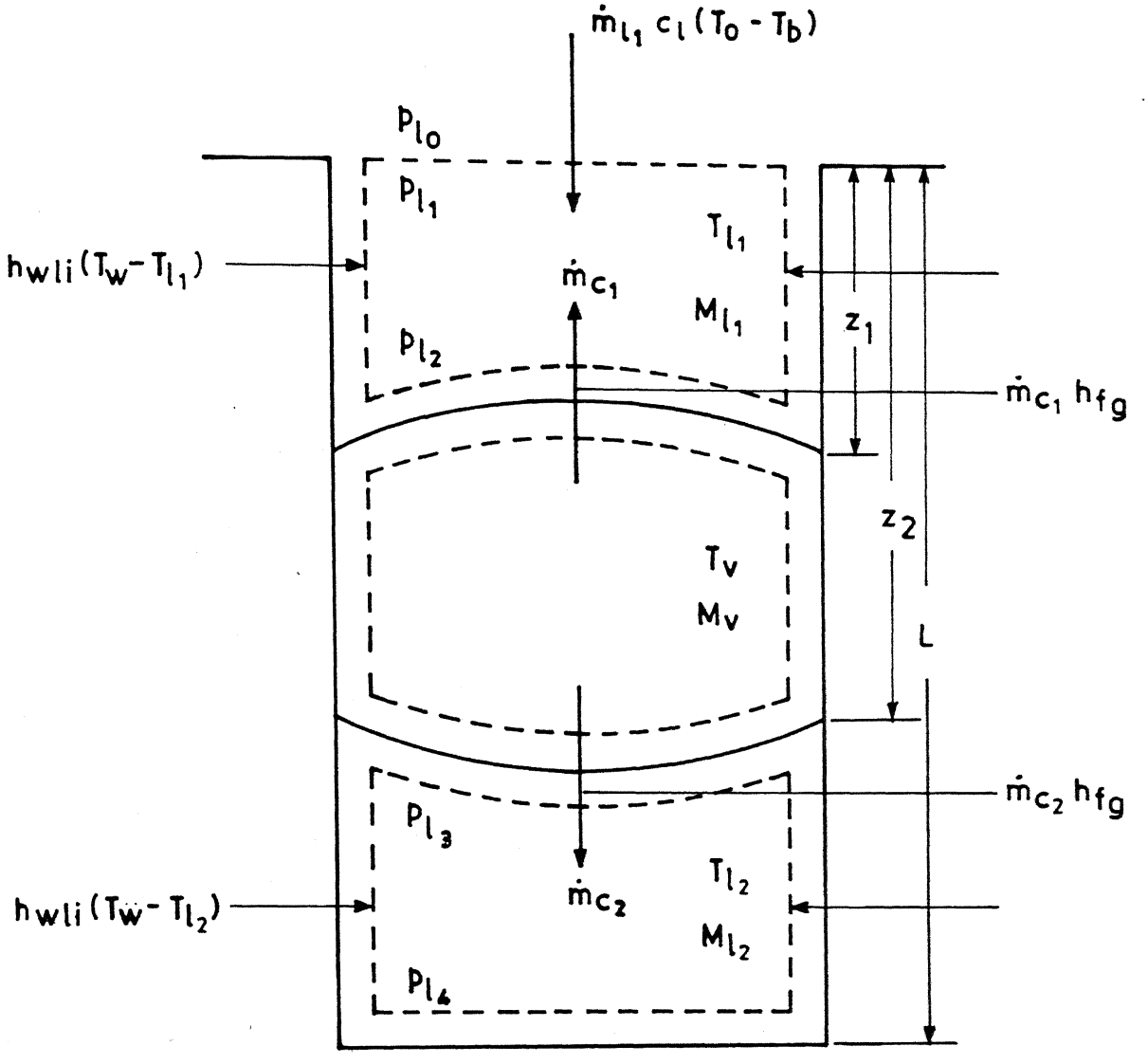

Fig. 4.3 Energy quantities for the liquid control volumes during the condensation phase.

Transfer of heat from the cavity walls

$$= A_{wli_1} \, h_{wli}(T_w - T_{1_1}) \tag{4.38}$$

The expansion work due to expansion of the ULCV

$$= \frac{1}{J} \, p_{1_2} \, \frac{d}{dt} \left[\frac{\pi D_c^2}{4} \, z_1\right] \tag{4.39}$$

Change in internal energy of the ULCV

$$= \frac{d}{dt} \, (M_{1_1} \, u_1) = \frac{d}{dt} \, [M_{1_1} \, c_1 (T_{1_1} - T_b)] \tag{4.40}$$

The heat balance over the ULCV yields,

$$\dot{m}_{1_1} \, c_1 (T_o - T_b) + \dot{m}_{c_1} c_1 (T_{1_1} - T_b) + A_{ic} \, h'_{ic} (T_v - T_{1_1}) + A_{wli_1} \, h_{wli} (T_w - T_{1_1}) = \frac{1}{J} \, p_{1_2} \, \frac{d}{dt} \left[\frac{\pi D_c^2}{4} \, z_1\right] + \frac{d}{dt} \, [M_{1_1} \, c_1 \, (T_{1_1} - T_b)] \tag{4.41}$$

Putting $A_i \, h'_{ic}(T_v - T_{1_1}) + \dot{m}_{c_1} \, c_1 \, (T_{1_1} - T_b) = A_i h_{ic} (T_v - T_{1_1})$ (4.42)

$$A_{wli_1} = \pi D_c z_1 \tag{4.43}$$

Using equation (4.42) and substituting the values of A_i, A_{wli}, $\dot{m}_{1_1}$ and M_{1_1} from equations (4.11), (4.43), (4.13) and (4.4) into equation (4.41) and simplifying yields

$$\frac{dT_{1_1}}{dt} = \frac{4z_1 h_{wli}(T_w - T_{1_1})}{D_c \rho_1 c_1 [z_1 - \frac{4V_{sc}}{\pi D_c^2}]} + \frac{2h_{ic}(T_v - T_{1_1})}{(1+\sin\theta)\rho_1 c_1 [z_1 - \frac{4V_{sc}}{\pi D_c^2}]}$$

$$+ \frac{V_1(T_o - T_b)}{[z_1 - \frac{4V_{sc}}{\pi D_c^2}]} - \frac{1}{[z_1 - \frac{4V_{sc}}{\pi D_c^2}]} [(T_{1_1} - T_b) + \frac{p}{J \rho_1 c_1}] \frac{dz_1}{dt} \quad (4.44)$$

Considering now the LLCV as shown in Fig. 4.3.

Sensible heat of the condensate going into the LLCV

$$= \dot{m}_{c_2} c_1 (T_{1_2} - T_b) \quad (4.45)$$

Heat transfer from the vapor to the LLCV through the interface (LLVI)

$$= A_i \; h'_{ic} (T_v - T_{1_2}) \quad (4.46)$$

Transfer of heat from the cavity walls,

$$= A_{wli_2} \; h_{w\,li} (T_w - T_{1_2}) \quad (4.47)$$

The expansion work due to the expansion of the LLCV

$$= \frac{1}{J} p_{1_3} \frac{d}{dt} [\frac{\pi D_c^2}{4} (L - z_2)] \quad (4.48)$$

Change in internal energy of the LLCV

$$= \frac{d}{dt} [M_{1_2} c_1 (T_{1_2} - T_b)] \quad (4.49)$$

The heat balance over the LLCV yields,

$$\dot{m}_{c_2} c_1 (T_{1_2}-T_b) + A_i \; h'_{ic} (T_v-T_{1_2}) + A_{wli_2} h_{wli}(T_w-T_{1_2})$$

$$= \frac{d}{dt} [M_{1_2} c_1 (T_{1_2}-T_b)] + \frac{1}{J} p_{1_3} \frac{d}{dt} [\frac{\pi D_c^2}{4} (L-z_2)] \qquad (4.50)$$

Putting $\dot{m}_{c_2 c1} (T_{1_2}-T_b) + A_i \; h'_{ic}(T_v-T_{1_2})$

$$= A_i \; h_{ic} (T_v-T_{1_2}) \qquad (4.51)$$

and

$$A_{wli_2} = \pi D_c (L-z_2) \qquad (4.52)$$

Using equation (4.51) and substituting the values of A_i, A_{wli_2} and M_{1_2} from equation (4.11), (4.52) and (4.5) into equation (4.50), one obtains

$$\frac{dT_{1_2}}{dt} = \frac{2h_{ic} (T_v - T_{1_2})}{(1+\sin\theta) \rho_1 c_1 [(L-z_2) - \frac{4V_{sc}}{\pi D_c^2}]}$$

$$+ \frac{4h_{wli}(L-z_2) (T_w-T_{1_2})}{D_c \rho_1 c_1 [(L-z_2) - \frac{4V_{sc}}{\pi D_c^2}]}$$

$$+ \frac{1}{[(L-z_2) - \frac{4V_{sc}}{\pi D_c^2}]} [(T_{1_2}-T_b) + \frac{p_{13}}{J\rho_1 c_1}] \frac{dz_2}{dt} \qquad (4.53)$$

4.3.4 Initial Conditions

The liquid from the bulk rushes towards the site, immediately after a bubble departs from that site. This liquid penetrates to a certain extent into the cavity in a negligibly small time. At the moment of bubble departure i.e., at t = 0, there is a small amount of liquid* present at the bottom of the cavity. Both the ULVI and LLVI are spherical cap shaped whose height is given by (see Fig. 4.2) :

$$S = \frac{1}{2} D_c(\sec \theta - \tan \theta) \qquad (4.54)$$

The liquid that penetrates into the cavity is assumed to have mean velocity of V_1. Here a value of 1.0 m s^{-1} is taken in conformity with the observations of Anton and Vekas (1973). The velocity of the LLVI and hence the induced velocity of the liquid in the LLCV, V_2, is assumed to be zero at t = 0.

The liquid that rushes into the cavity and enters the ULCV may come partly from the bulk and partly from the thermal layer. The temperature of the liquid within the ULCV, T_{1_1}, may be such that at t = 0, $T_b \leq T_o < T_w$.

*The presence of this liquid can be clearly seen from the photographic data of Kant (1983). It may either be present due to the flow of bulk liquid to the cavity bottom at the moment of departure or it may be present to maintain a contact angle θ for the given surface-liquid combination.

The liquid at a temperature, T_{1_2}, present in the LLCV is assumed to be cooled to T_s, possibly due to the penetration of the bulk liquid into it at the moment of bubble departure (i.e., at t = 0).

The positive direction is taken into the cavity and the coordinates z_1 and z_2 measure the distances of the ULVI and LLVI at any time t from the mouth of the cavity.

The initial conditions for the condensation phase can be summarized as follows :

At t = 0

$$z_1 = S$$

$$z_2 = L-S$$

$$V_1 = V_{o_1} \qquad 0 \leq V_o \leq 1 \qquad (4.55)$$

$$V_2 = 0$$

$$T_{1_1} = T_o \qquad T_b \leq T_o \leq T_w$$

$$T_{1_2} = T_s$$

Condensation phase is considered to be complete as soon as $T_{1_1} = T_{1_2} = T_v$. If any of the liquid temperatures reach the value of T_v earlier, it is taken to be constant until the other liquid temperature reaches T_v. Equations (4.14), (4.17), (4.29), (4.33), (4.44) and (4.53) were solved numerically subjected to the initial conditions given by equation (4.55) to determine the condensation time t_c.

4.4 FIRST EVAPORATION PHASE

When the condensation phase is complete, any additional heat transfer from the cavity walls will mostly go to evaporate the liquid at the ULVI and LLVI causing reversal of their motion. The first evaporation is assumed to be over when the top of the ULVI is even with the surface, i.e., $z_1 = S$. By this time, the LLVI reaches its maximum value, $z_2 = L-S$. The liquid present in both the ULCV and LLCV are at the vapor temperature T_v.

4.4.1 Mass Balances

During the upward motion of the ULVI, some liquid will flow out of the cavity. During this period, the LLVI will move downwards until it almost reaches the bottom of the cavity. The mass balances over the ULCV and LLCV shown in Fig. 4.4, yield

$$-\dot{m}_{12} - \dot{m}_{e_1} = \frac{dM_{1_1}}{dt} \tag{4.56}$$

$$\dot{m}_{e_1} + \dot{m}_{e_2} = \frac{dM_v}{dt} \tag{4.57}$$

$$-\dot{m}_{e_2} = \frac{dM_{1_2}}{dt} \tag{4.58}$$

where $\dot{m}_{e_1}$ and $\dot{m}_{e_2}$ denote the rate of liquid evaporation at the interfaces and $\dot{m}_{12}$ rate mass outflow from the cavity. Adding equations (4.56), (4.57) and (4.58) and using equations (4.4), (4.5) and (4.6) yields

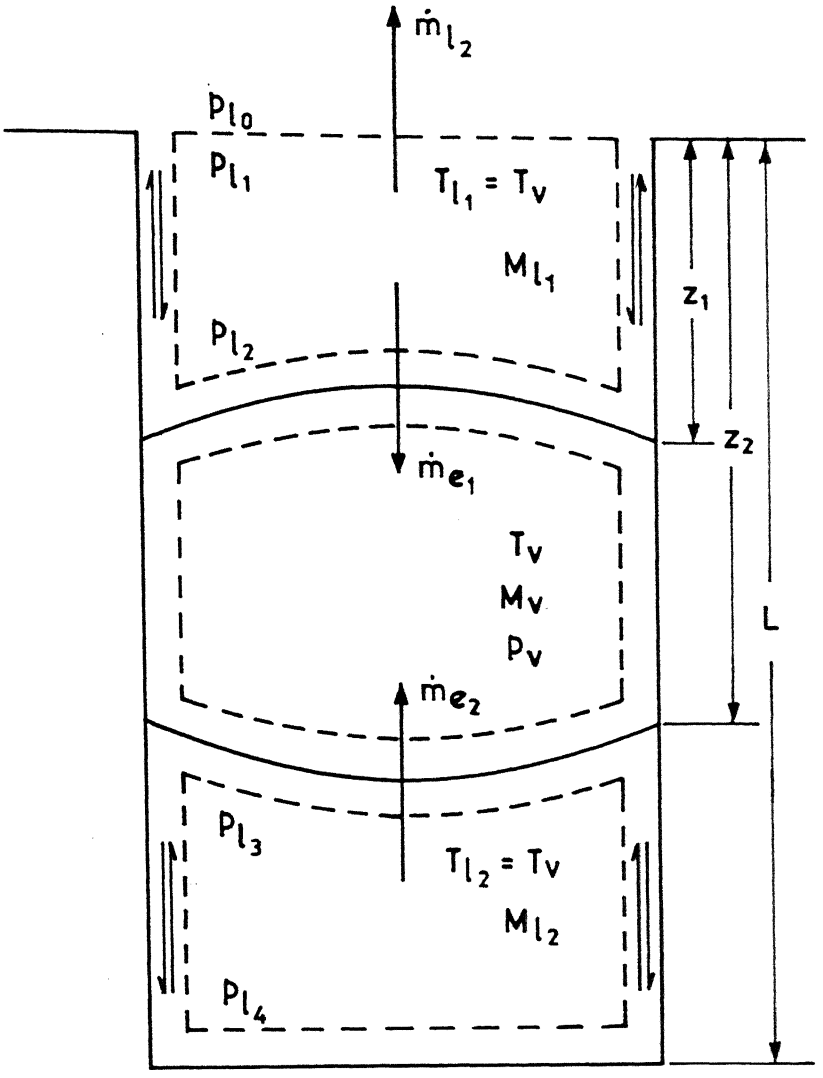

Fig. 4.4 Liquid and vapor control volumes within a cavity during the first evaporation phase.

$$-\dot{m}_{1_2} = \frac{\pi D_c^2}{4} (\rho_1 - \rho_v) \left[\frac{dz_1}{dt} - \frac{dz_2}{dt}\right] \tag{4.59}$$

4.4.2 Momentum Balances

The momentum balance over the upper liquid control volume shown in Fig. 4.3 yields

$$-(p_{1_2} - p_{1_1}) \frac{\pi D_c^2}{4} + \left(\frac{\pi D_c^2}{4} z_1 - V_{sc}\right) \rho_1 g + \pi D_c z_1 \tau_w$$

$$= \frac{\pi D_c^2}{4} \rho_1 (-V_1) \frac{dz_1}{dt} + \frac{d}{dt} \left[\frac{\pi D_c^2}{4} z_1 - V_{sc}\right] \rho_1 V_1 \tag{4.60}$$

Rewriting the above equation

$$\frac{dV_1}{dt} = g + \frac{1}{\left[z_1 - \frac{4V_{sc}}{\pi D_c^2}\right]\rho_1} \left[(p_{1_1} - p_{1_2}) + \frac{4 z_1 \tau_w}{D_c}\right] \tag{4.61}$$

a. Pressure Loss due to sudden expansion

There is a head or pressure loss h_{1e} due to sudden expansion involved when the liquid flows out of the cavity mouth, and it is given by

$$h_{1e} = C_e \frac{V^2}{2g} \text{ meter of fluid} \tag{4.62}$$

where C_e is the coefficient of expansion approximately equal to unity. This can be written as

$$h_{1e} = C_2 V_1^2 \tag{4.63}$$

where $C_2 = 1.333224 \times 10^5 \left(\frac{C_e}{2g}\right)\left(\frac{\rho_1}{\rho_{Hg}}\right)$ (4.64)

The pressure, p_{1_1}, can be written as

Therefore, $p_{1_1} = p_{1_o} + C_2 V_1^2$ (4.65)

b. Wall Shear Stress

The wall shear stress for the Hagen-Poiseuille flow using the velocity distribution given by equation (4.27) is given by

$$(\tau_w)_{HP} = -\frac{8V_1\mu}{D_c} \tag{4.66}$$

Substituting the values of p_{1_1}, and τ_w from equations (4.65) and (4.66) respectively, one obtains

$$\frac{dV_1}{dt} = g + \frac{1}{\left[z_1 - \frac{4V_{sc}}{\pi D_c^2}\right]\rho_1}\left[(p_{1_o} + C_2 V_1^2 - p_{1_2}) - \frac{32V_1\mu z_1}{D_c^2}\right] \tag{4.67}$$

The momentum balance over the LLCV shown in Fig. 4.3 yields,

$$-(p_{1_3} - p_{1_4})\frac{\pi D_c^2}{4} + \left[\frac{\pi D_c^2}{4}(L-z_2) - V_{sc}\right]\rho_1 g - \pi D_c (L-z_2)\tau_w$$

$$= \frac{d}{dt}\left[\frac{\pi D_c^2}{4}(L-z_2) - V_{sc}\right]\rho_1 V_2 \tag{4.68}$$

Substituting $\tau_w = \frac{8V_2\mu}{D_c}$ in the above equation and simplifying gives

$$\frac{dV_2}{dt} = g - \frac{1}{\left[(L-z_2) - \frac{4V_{sc}}{\pi D_c^2}\right]\rho_1}\left[(p_{1_3} - p_{1_4}) + \frac{32V_2\mu(L-z_2)}{D_c} - \rho_1 V_2 \frac{dz_2}{dt}\right] \tag{4.69}$$

4.4.3 Energy Balance

During the evaporation phase, the liquid temperatures, T_{1_1}, and, T_{1_2}, in the ULCV and LLCV are already at the vapor temperature, T_v, and there is no heat transfer across the l-v interfaces. For computing the energy quantities for the control volumes, T_b is taken as the reference temperature.

Consider the ULCV as shown in Fig. 4.5.

Sensible heat of the liquid leaving the ULCV

$$= \dot{m}_{1_2} c_1 (T_v - T_b) \tag{4.70}$$

Heat of vaporization of the mass leaving the ULCV

$$= \dot{m}_{e_1} h_{fg} \tag{4.71}$$

Transfer of heat from the cavity walls

$$= A_{wli_1} h_{wli} (T_w - T_v) \tag{4.72}$$

The flow work due to contraction of the liquid control volume

$$= \frac{1}{J} p_{1_2} \frac{\pi D_c^2}{4} \frac{dz_1}{dt} \tag{4.73}$$

where $\frac{dz_1}{dt}$ is a negative quantity.

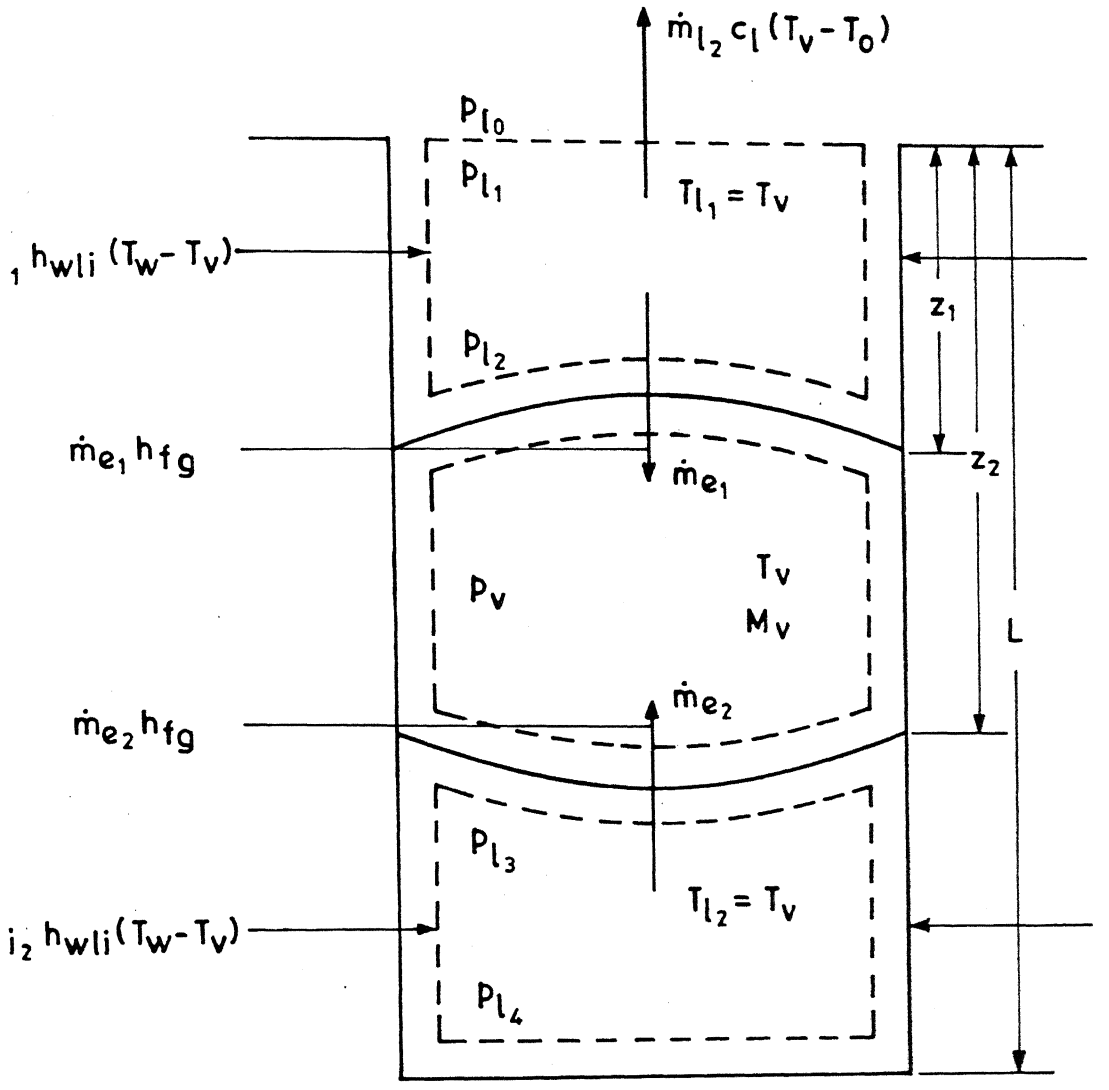

Fig. 4.5 Energy quantities for the liquid control volume during the first evaporation phase.

Change in internal energy of the ULCV

$$\Delta U_1 = \frac{d}{dt}(M_{1_1} u) = M_{1_1}\frac{du}{dt} + u\frac{dM_{1_1}}{dt}$$

$$= M_{1_1} c_1 \frac{dT_v}{dt} + c_1 (T_v - T_b)\frac{dM_{1_1}}{dt} \qquad (4.74)$$

$c_1 dT_v = 0$ as T_v = constant.

Energy balance over the ULCV yields

$$-\dot{m}_{1_2} c_1 (T_v - T_b) - \dot{m}_{e_1} h_{fg} + A_{wli_1} h_{wli} (T_w - T_v)$$

$$= C_1 (T_v - T_b), \frac{dM_{1_1}}{dt} + \frac{1}{J} p_{1_2} \frac{\pi D_c^2}{4}\frac{dz_1}{dt} \qquad (4.75)$$

where

$$A_{wli_1} = \pi D_c z_1 \qquad (4.76)$$

and using equations (4.57) and (4.58) $\dot{m}_{e_1}$ can be written as

$$\dot{m}_{e_1} = \frac{dM_v}{dt} - \dot{m}_{e_2} = \frac{dM_v}{dt} + \frac{dM_{1_2}}{dt}$$

which upon using equations (4.5) and (4.6) gives

$$-\dot{m}_{e_1} = + \frac{\pi D_c^2}{4}\left[\rho_v \frac{dz_1}{dt} + (\rho_1 - \rho_v)\frac{dz_2}{dt}\right] \qquad (4.77)$$

Substituting the values of A_{wli_1}, $\dot{m}_{1_2}$, $\dot{m}_{e_1}$ and M_{1_1} from equations (4.76), (4.59), (4.77) and (4.4) respectively, into equation (4.77) and simplifying yields

$$\frac{dz_1}{dt} = \frac{1}{\left[\frac{p_{1_2}}{J} + \rho_v c_1 (T_v - T_b) - \rho_v h_{fg}\right]} \left\{\left[h_{fg}(\rho_1 - \rho_v) - c_1(\rho_1 - \rho_v)(T_v - T_b)\right] \frac{dz_2}{dt} + \frac{4 z_1 h_{wli}}{D_c} (T_w - T_v)\right\} \quad (4.78)$$

Consider now the LLCV.

Heat of vaporization of the mass leaving the lower control volume

$$= \dot{m}_{e_2} h_{fg} \quad (4.79)$$

Heat transfer from the cavity walls to the liquid

$$= A_{wli_2} h_{wli} (T_w - T_v) \quad (4.80)$$

The flow work due to the contraction of the LLCV

$$= \frac{1}{J} p_{1_3} \frac{\pi D_c^2}{4} \frac{d}{dt} (L - z_2) \quad (4.81)$$

Change in internal energy of the lower control volume

$$\Delta U_2 = \frac{d}{dt} (M_{1_2} u)$$

$$= M_{1_2} c_1 \frac{dT_v}{dt} + c_1 (T_v - T_b) \frac{dM_{1_2}}{dt}$$

$$= c_1 (T_v - T_b) \frac{dM_{1_2}}{dt} \quad (4.82)$$

Energy balance over the LLCV yields

$$-\dot{m}_{e_2} h_{fg} + A_{wli_2} h_{wli} (T_w - T_v) = \frac{1}{J} p_{1_3} \frac{\pi D_c^2}{4} \frac{d}{dt} (L - z_2) + c_1 (T_v - T_b) \frac{dM_{1_2}}{dt} \qquad (4.83)$$

Substituting for $\dot{m}_{e_2}$, M_{1_2} and A_{wli_2} from equations (4.58), (4.5), and (4.52) into equation and simplifying yields

$$\frac{dz_2}{dt} = \frac{1}{[\rho_v h_{fg} - \frac{p_{1_3}}{J} - \rho_1 c_1 (T_v - T_b)]} \left[\frac{4 h_{wli} (L - z_2)(T_w - T_v)}{D_c}\right] \qquad (4.84)$$

4.4.4 Initial Conditions

The conditions at the end of the condensation phase are the initial conditions for the first evaporation phase.

$$\text{At } t = t_c \qquad \begin{aligned} z_1 &= z_{c1} \\ z_2 &= z_{c2} \\ V_1 &= V_{mc_1} \\ V_2 &= V_{mc_2} \end{aligned} \qquad (4.85)$$

Equations (4.78), (4.84), (4.67) and (4.69) were solved, Numerically subject to the initial conditions given by equation (4.85) to determine the time t_{e_1} corresponding to $z_1 = S$.

4.5 SECOND EVAPORATION PHASE

During this phase, it is assumed that heat is transferred in the axial direction as well as radially from the cavity walls. For the vapor nucleus to appear above the surface, an additional time t_{e_2} must elapse before z_l becomes equal to zero. The liquid present at the bottom of the cavity is assumed to play no role during this phase.

The surface area of the spherical segment above the heating surface, as shown in Fig. 4.6, is given by

$$A_{im} = 2\pi R_i (S - z_l) \tag{4.86}$$

Assuming that the liquid temperature at the cavity mouth at $t = t_{e_l}$ equals the wall temperature T_w, the rate of evaporation at the ULVI is

$$\dot{m}_{e_l} = \frac{\pi D_c z_l h_{wli} (T_w - T_v) + A_{im} h_{ie} (T_w - T_v)}{h_{fg}} \tag{4.87}$$

where

h_{ie} = film heat transfer coefficient for the evaporating ULVI (assumed equal to h_{ic})

Substituting for A_{im} from equation (4.86) and writing $R_i = \frac{R_c}{\cos \theta}$ into equation (4.87), yields

$$\dot{m}_{e_l} = \frac{\pi D_c (T_w - T_v)}{h_{fg}} \left[\left(h_{wli} - \frac{h_{ie}}{\cos \theta} \right) z_l + \frac{S h_{ie}}{\cos \theta} \right] \tag{4.88}$$

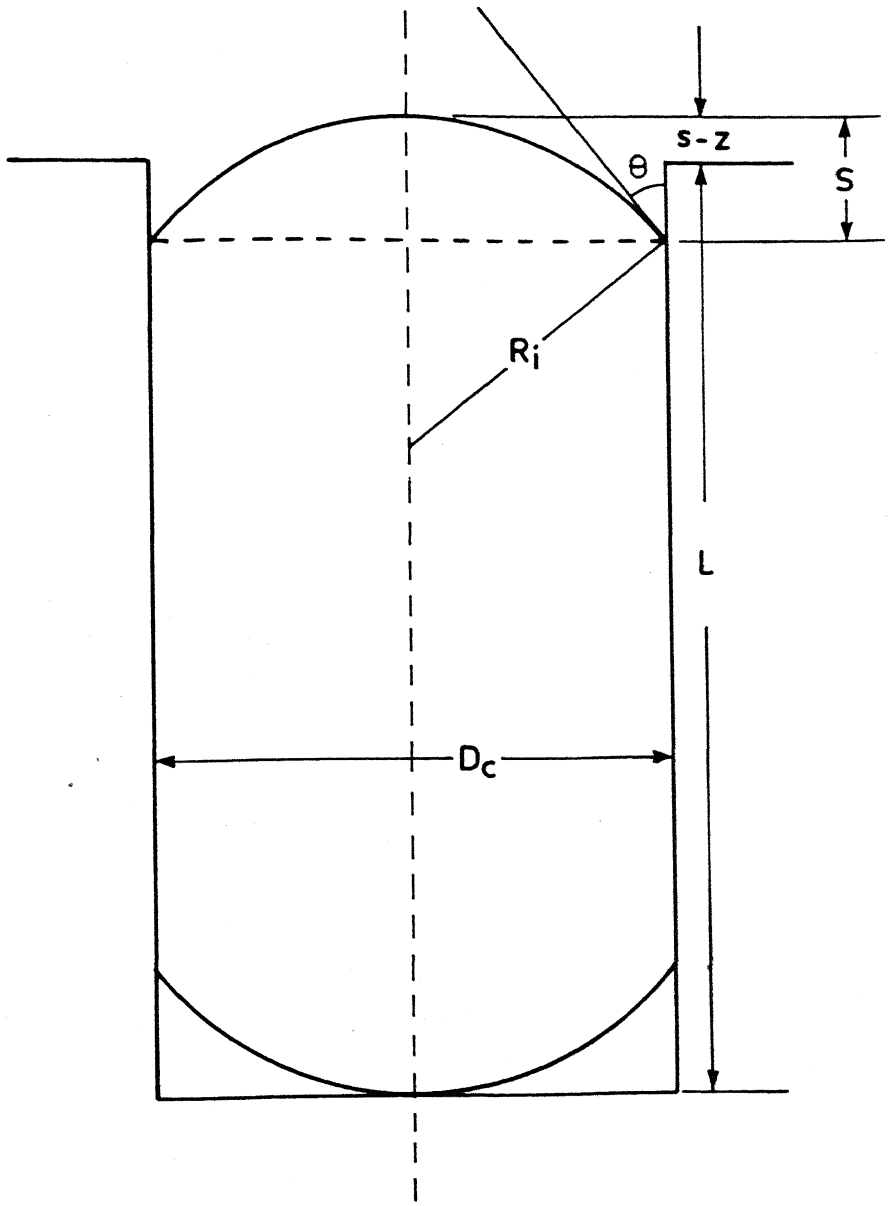

Fig. 4.6 l - v interface protruding from a cavity during the second evaporation phase.

Using equation (4.77) and assuming $(dz_2/dt) = 0$, yields

$$\frac{dz_1}{dt} = -\frac{4(T_w - T_v)}{D_c \; v h_{fg}} \left[\left(h_{wli} - \frac{h_{ie}}{\cos \theta} \right) z_1 + \frac{S h_{ie}}{\cos \theta} \right] \qquad (4.89)$$

The momentum equation for the second evaporation phase is the same as equation (4.67).

Initial Conditions

The conditions at the end of the first evaporation phase are the initial conditions for the second evaporation phase.

At $t = t_{e_1}$

$$z_1 = S$$

$$V_1 = V_{me_1} \qquad (4.90)$$

4.6 PREDICTIONS

The model equations for each of the three phases, developed in the preceding sections were solved numerically to predict the waiting time of a bubble for given boiling conditions. The method of solution of the equations is described in Appendix C.

The equations were used for both subcooled and saturated pool boiling.

4.6.1 Application of the Model

The solution of the equations involved the values of h_{ie} and h_{wli} which were calculated using equations (D.1) and (D.2). The multipliers M_1 and M_2 were chosen for water to agree with the

available frequency data of Shoukri and Judd (1978). The waiting time was taken as 75% of the bubble cycle period. In accordance with the measurements of Shoukri, the contact angle for water boiling on a copper surface was taken to be 22^{o}. For isopropanol, the contact angle was taken as 10^{o} and M_2 was related to that for water through a ratio of thermal conductivities (Kant, 1983) as

$$M_2 = (k_l / k_{l_r})^{1.25} M_{2r} \qquad (4.91)$$

where M_2 and k_l represent the multiplier and the thermal conductivity for isopropanol and M_{2r} and k_{l_r} are the same for the reference liquid which was taken as water here. The values of M_1 and M_2 for both the liquids are given in Table 4.1.

Table 4.1

Multipliers for h_{ic} and h_{wli}

Boiling Liquid	M_1	M_2
Water	1×10^{-4}	5×10^{-3}
Isopropanol	1×10^{-4}	7×10^{-4}

4.6.2 HPB of Water and Isopropanol

The model equations were solved numerically for both water and isopropanol. The various parameters were computed as a function of time. The properties used for the various liquids are tabulated in Appendix A. The solution of equations predicted the waiting time as a function of cavity diameter, cavity-depth, degree of superheat, (T_w-T_s), and the degree of subcooling, (T_s-T_b).

The predictions for two different cases of subcooling and different degrees of superheat for water are given in Tables 4.2 and 4.3. Table 4.4 gives the predictions for the saturated boiling of isopropanol. These tables also give the computed values of S, p_v, T_v, h_{ic}, h_{wli}, z_{c1} and z_{c2}.

The positions of the ULVI and LLVI at different times are shown in Fig. 4.7. It is seen that the ULVI penetrates into the cavity to its maximum value, $z_l = z_{cl}$, within a fraction of a millisecond. The reversal of velocity from positive to negative takes place as soon as $z_l = z_{cl}$ is reached and then z_l slightly decreases. The ULVI stays at this position, more or less, throughout the condensation phase, i.e., until the liquid temperature T_{l_1} reaches the vapor temperature, T_v. Once this condition is reached the first evaporation phase begins during which the ULVI rises up in the cavity to a value $z_l = S$. This phase lasts for a fraction of a

TABLE 4.2

Effect of Cavity Size and Degree of Superheat on Bubble Waiting Time

V_o = 1.0 ms^{-1} $\quad$ p_{l_o} = 1.01325 x 10^5 $N.m^{-2}$

T_s = 373.15 K $\quad$ θ = 22°

C_1 = 239.43 $\quad$ $T_s - T_b$ = 2.2 K

C_2 = 478.86 $\quad$ Liquid = water

D_c µm	L µm	S µm	p_v mm Hg	T_v K	$h_{lic_2K^{-1}}$ $Wm^{-2}K^{-1}$	h_{wli} $Wm^{-2}K^{-1}$	$T_w - T_s$ K	z_{c_1} µm	z_{c_2} µm	t_c ms	t_{e_1} ms	t_{e_2}	t_w ms	t_w experimental ms
1	2	3	4	5	6	7	8	9	10	11	12	13	14	15
12	50	4.1	896.1	378.56	839.0	1040.2	5.9	14.8	45.9	22.0	0.2	8.8	31.0	
							10.9	14.8	45.9	8.0	0.16	0.8	8.96	18.3, 15.3
							20.9	14.8	45.9	4.0	0.12	0.4	4.52	
20	75	6.7	841.65	376.40	799.6	624.1	5.9	39.7	68.2	29.2	0.4	3.6	33.2	
							10.9	39.7	68.2	14.8	0.36	1.2	16.36	
							15.9	39.7	68.2	10.4	0.32	0.8	11.52	
							20.9	39.7	68.2	8.0	0.28	0.8	9.08	
40	240	13.5	800.82	374.77	769.2	312.1	5.9	158.9	226.4					
							10.9	158.9	226.4	40.8	0.52	2.8	44.12	
							15.9	158.9	226.4	28.8	0.52	2.0	31.32	
							20.9	158.9	226.4	22.0	0.48	1.6	24.08	

TABLE 4.3

Effect of Cavity Size and Degree of Superheat on Bubble Waiting Time

V_o = 1 ms^{-1} $\quad$ p_{l_o} = 1.01325 x 10^5 Nm^{-2}

T_s = 373.15 K $\quad$ θ = 22°

C_1 = 239.43 $\quad$ $T_s - T_b$ = 1.2 K

C_2 = 478.86 $\quad$ Liquid = water

D_c µm	L µm	S µm	P_v mm Hg	T_v K	h_{ic} $Wm^{-2}K^{-1}$	h_{wli} $Wm^{-2}K^{-1}$	$T_w - T_s$ K	z_{c_1} µm	z_{c_2} µm	t_c ms	t_{e_1} ms	t_{e_2} ms	t_w ms	t_w experimental ms
1	2	3	4	5	6	7	8	9	10	11	12	13	14	15
12	50	4.1	860.1	378.56	839.0	1040.2	5.9	14.8	45.9	21.6	0.2	8.8	30.6	
							10.9	14.8	45.9	7.6	0.16	0.8	8.56	
							20.9	14.8	45.9	3.6	0.12	0.4	4.12	
20	76	6.7	841.65	376.40	799.6	624.1	5.9	39.7	68.2	26.4	0.4	3.6	30.4	
							10.9	39.7	68.2	13.2	0.36	1.2	14.76	
							15.9	39.7	68.2	8.8	0.32	0.8	9.92	
							20.9	39.7	68.2	6.8	0.28	0.8	7.88	
40	240	13.5	800.82	374.77	769.2	312.1	5.9	158.9	226.4	59.2	0.56	6.4	66.16	
							10.9	158.9	226.4	32.0	0.52	2.8	35.32	
							15.9	158.9	226.4	22.0	0.52	2.0	24.52	
							20.9	158.9	226.4	16.8	0.48	1.6	18.88	

TABLE 4.4

Effect of Cavity Radius and Degree of Superheat on the Waiting Time

V_o = 1.0 ms^{-1} p_{l_o} = 1.01325 x 10^5 Nm^{-2}

T_s = 355.4K θ = 10°

C_1 = 183.34 $T_s - T_b$ = 0.0

C_2 = 366.69 Liquid = Isopropanol

D_c	L	S	P_v	T_v	h_{ic}	h_{wli}	$T_w - T_s$	z_{c_1}	z_{c_2}	t_c	t_{e_1}	t_{e_2}	t_w	t_w experimental
µm	µm	µm	mm Hg	K	$Wm^{-2}K^{-1}$	$Wm^{-2}K^{-1}$	K	µm	µm	ms	ms	ms	ms	ms
1	2	3	4	5	6	7	8	9	10	11	12	13	14	15
12	50	5	807.3	357.06	463.5	30.7	9.2	8.6	44.9	13.6	1.88	3.6	19.08	
							19.2	8.6	44.9	9.6	0.28	1.6	11.48	
20	75	8.4	788.4	356.40	454.8	18.4	9.2	19.6	66.6	31.2	0.56	6.4	38.16	
							14.2	19.6	66.6	23.2	0.6	4.0	27.80	
							19.2	19.6	66.6	18.4	0.6	2.8	21.80	
40	240	16.8	774.17	355.90	448.2	9.2	9.2	69.8	223.1	79.6	0.76	14.0	94.36	
							14.2	69.8	223.1	58.4	0.84	8.8	68.04	
							19.2	69.8	223.1	46.0	0.84	6.4	53.24	

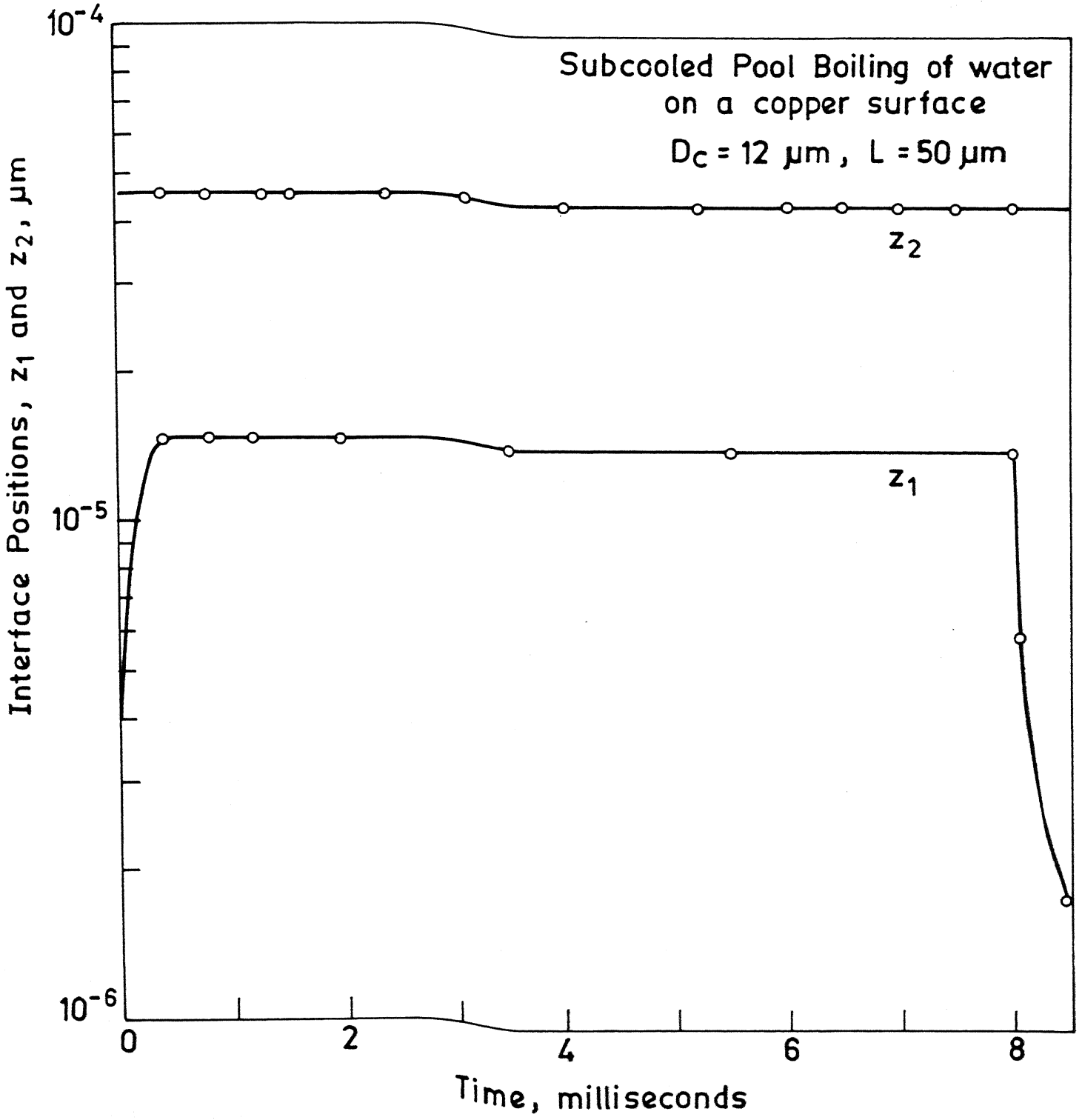

Fig. 4.7 Variation of ULVI and LLVI positions with time.

millisecond. The second evaporation phase begins as soon as z_1 becomes equal to S and the ULVI rises further up towards the cavity mouth until z_1 becomes equal to zero and the vapor nucleus protrudes out of the cavity.

The LLVI during the whole cycle is more or less at the bottom of the cavity where $z_2 = L-S$.

During the condensation phase, the velocity, V_1, drops to a small value in a fraction of a millisecond and turns negative and shows a slight increase in the value. The velocity, V_2, rises upto a few milliseconds in the negative direction and then stays constant at a negligibly small value.

The variation of temperatures T_{l_1} and T_{l_2} are shown in Fig. 4.8. The temperatures of the liquid present in the ULCV and LLCV, increases steadily during the condensation phase until they become equal to the vapor temperature. The liquid in the ULCV takes a longer time to attain the vapor temperature than the liquid in the LLCV. The temperatures T_{l_1} and T_{l_2} remain at T_v during the evaporation phases.

4.6.3 Effect of Model Parameters

a. Cavity Diameter

The predicted waiting time increases as the cavity diameter, D_c increases. This is because more liquid from the bulk, flows into the cavity which then takes a longer time to heat up

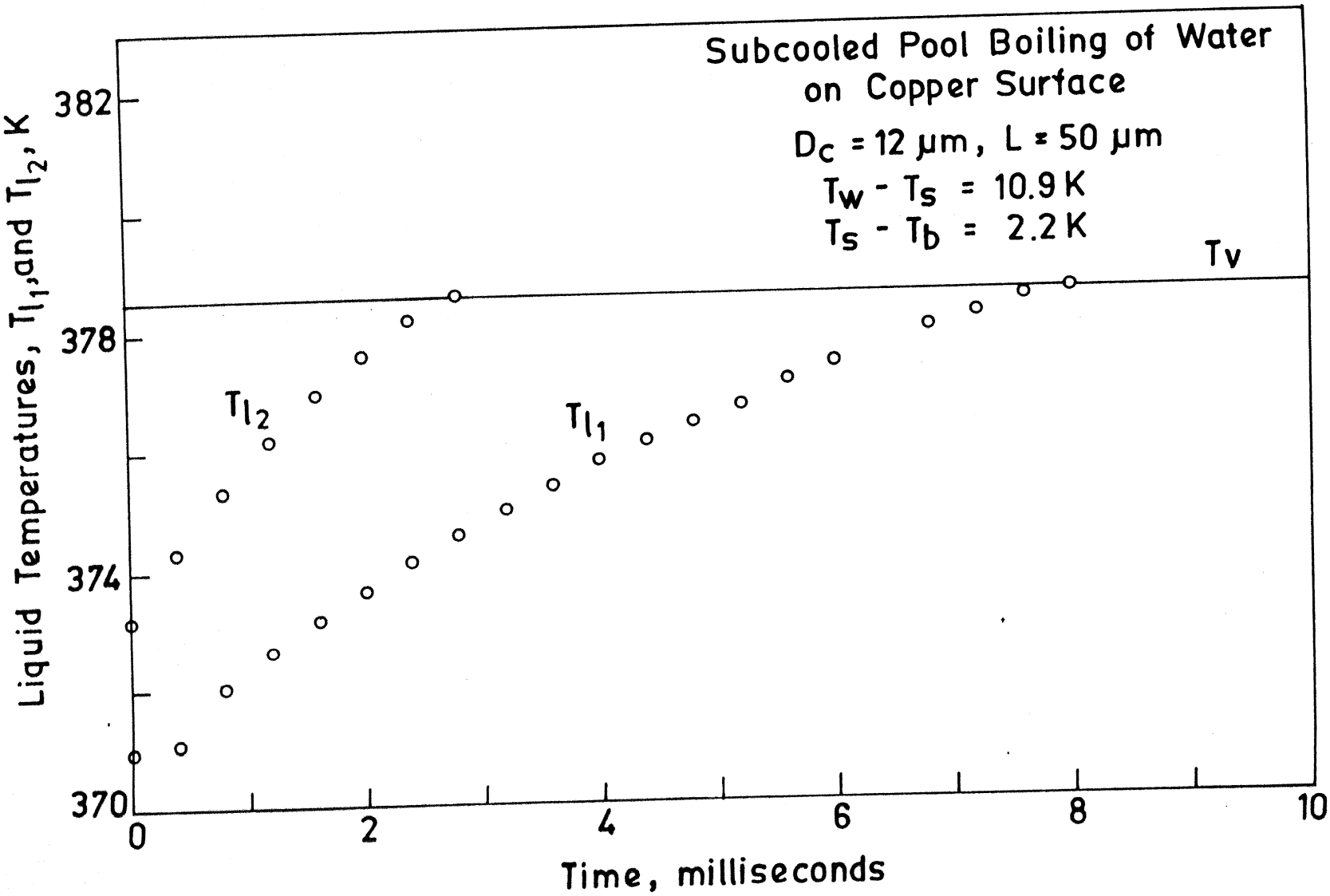

Fig. 4.8 Variation of liquid temperatures within the control volume with time.

to the vapor temperature. Also as D_c increases; p_v, T_v, h_{ic} and h_{wli} decrease which result in reduced rate of heat transfer into the cavity, and larger depth of penetration thereby increasing the waiting time.

As shown in Tabld 4.2, theoretically predicted value of the waiting time is in good agreement with the experimental value.

b. Degree of Superheat

Tables 4.2, 4.3 and 4.4 also show the computations for various values of degree of superheat. An increase in its value increases the heat transfer rate and thereby results in a lower waiting time. It can also be seen that the depth of penetration is not significantly dependent upon the degree of superheat.

c. Degree of Subcooling

A larger degree of subcooling increases the predicted waiting time, but the depth of penetration is not affected by it (see Tables 4.2 and 4.3).

4.6.4 Stability of Nucleation Sites

The model equations presented earlier relate all the relevant parameters of boiling nucleation phenomena. Computations for given boiling conditions as shown in Tables 4.2, 4.3 and 4.

show clearly that it is only the cavity size which controls z_1 and z_2. Whether or not a cavity is a stable nucleation site, will depend upon the value of L/D_c. If $(L/D_c) \leq 2.7$, $V_v \leq V_s$, and the cavity will get filled up with the boiling liquid.

CHAPTER 5

CONCLUSIONS

5.1 MODELING OF THERMAL LAYER THICKNESS

All the relevant parameters of N.B. were considered in developing an expression for δ_t. The dimensionless groups obtained were combined in an arbitrary manner to reduce the number of data points required to evaluate the indices ε_i ($i = 1, 4$). The results obtained are in good agreement with the values of δ_t reported in literature.

Unfortunately, there is no reliable experimental data on δ_t because of which only estimated values of δ_t for various liquids were used. The apparent limitation of the proposed expression is that some experimental data on δ_t is definitely required to evaluate the indices ε_i. But the dimensionless groups obtained could be combined into one or 2 groups if a very limited data are available.

5.2 BUBBLE NUCLEATION SUPERHEATS

Kant's (1983) bubble nucleation model was extended to incorporate a proposed TD given by equation (3.14). Substitution of various parameters in equation (3.18) and the constants given in Table 3.2 resulted in Nucleation Superheats somewhat higher than those predicted by Kant, and naturally in better

agreement with the experimental values. These superheats give a stability criterion for the nucleation of a bubble for a given size of a cavity.

5.3 SIZE RANGE OF ACTIVE SITES

The expressions developed for the bubble nucleation superheat related (T_w-T_s) to (T_e-T_s), R_c and θ. For given values of (T_w-T_s) and surface-liquid combination, the size of active nucleation site or its size range could be computed.

The predicted size range shown in Table 3.3 is wider than that predicted by Hsu (1962) and Han and Griffith (1965), but the minimum cavity radius, R_c, is more or less the same for a given degree of superheat. Values of predicted $R_{c_{min}}$ are slightly higher than those of Hsu, but slightly lower than those of Han and Griffith. As only the smaller cavities serve as active nucleation sites (Shoukri and Judd, 1975), the author is of the opinion that the prediction of the maximum size is not enough to say whether or not it will be an active site. Hence the predicted maximum size is basically of no use until its geometry etc. is specified.

5.4 DYNAMIC MODEL AND NUCLEATION SITE STABILITY

Based upon the bubble nucleation and site deactivation mechanisms proposed by Kant (1983), a dynamic model was develo ped to simulate the HPB of liquids on single sites in a natura

surface and evolve criteria for the stability of these sites.

Kant's experiments clearly exhibited the presence of some liquid at the bottom of the cavity and thus in an active nucleation site, there was liquid present at the top and the bottom and a vapor bubble was stuck in the middle. This provided the l-v interfaces at the top and bottom (ULVI and LLVI). The model proposed here for the first time took into account the condensation and evaporation at both of these interfaces to predict the waiting times of bubbles which were found to be in agreement with the available experimental data of Shoukri and Judd (1978). The predictions of the model also showed that the diameter and the depth of a cavity basically determined the stability of a nucleation site. Other variables like degrees of superheat and subcooling were not found to be important.

The model was applied to subcooled and saturated pool boiling.

REFERENCES

1. Anton, I., and Vekas, L., A study on the cavitation bubble formation process, Rev. Roum. Sci. Techn.Mec. Appl., 18, 6, pp 1113-1129, 1973.
2. Bankoff, S.G., The predictions of surface temperatures at incipient boiling, Chem. Eng. Prog. Symp. Ser., 55, 29, pp 87-94, 1959.
3. Clark, H.B., Strenge, P.S. and Westwater, J.W., Active sites for nucleate boiling, Chem. Eng. Prog. Symp.Ser., 55, pp 103-110, 1959.
4. Fabic, S., Vapor nucleation on surfaces subjected to transient heating, Ph.D. Thesis, Univ of California, 1964.
5. Griffith, P. and Wallis, J.D., The role of surface conditions in nucleate boiling, Chem. Eng. Prog. Symp. Ser., 56, 30, pp 49-63, 1960.
6. Han, C.Y., and Griffith, P., The mechanism of heat transfer in nucleate pool boiling - Part I, Bubble initiation, growth and departure, Int. J. of Heat and Mass Transfer,8, pp 887-904, 1965.
7. Howell, J.R., and Siegel, R., Activation, growth and detachment of boiling bubbles in water from artificial nucleation sites of known geometry and size, NASA TND-4101, 42 pages, 1967.

8. Hsu, Y.Y., On the size range of active nucleation cavities on a heating surface, J. of Heat Transfer, Trans. ASME, C84, 3, pp 207-216, 1962.

9. Hsu, Y.Y., and Graham, R.W., An analytical and experimental study of tie thermal boundary layer and Ebullition cycle in nucleate boiling, NASA TN D-594, 44 pages, 1961.

10. Kant, K., Models of boiling nucleation, Ph.D. Thesis, McGill University, 1983.

11. Kant, K. and Weber, M.E., Dynamic model for bubble nucleation in heterogeneous pool boiling of liquids,Part I - model equations, 1986a, to be published in J. Heat Transfer, ASME.

12. Kant, K., and Weber, M.E., Dynamic model for bubble nucleation in heterogeneous pool boiling of liquids,Part II - model predictions, 1986b, to be published in J. Heat Transfer, ASME.

13. Kant, K., and Weber, M.E., Stability of nucleation sites in pool boiling, 1986c, to be published in J. Heat Transfer, ASME.

14. Leont'ev, A.I., and Kirdyashkin, A.G., The theory of the convective heat transfer for the vertical heat transfer for the vertical flow of fluid, Proc. of the 3rd Int. Heat Transfer Conference, Chicago, 1, pp 216-224, 1966.

15. Lippert, T.E., and Dougall, R.S., A study of the temperature profiles measured in the thermal sublayer of water, Freon-113 and Methyl Alcohol during pool boiling, J. of Heat Transfer, Trans. ASME, C90, 3, pp 347-352, 1968.

16. Marcus, B.P., and Dropkin, D., Measured temperature profiles within the superheated boundary layer above a horizontal surface in a saturated nucleate pool boiling of water, J. of Heat Transfer, Trans. ASME, 87, pp 333-341, 1965.

17. Marto, P.J., and Rohsenow, W.M., Nucleate boiling instability of alkali metals, J. of Heat Transfer, Trans. ASME, C88, 2, pp 183-195, 1966.

18. Perry, R.H., and Chilton, C.H., Chemical engineers handbook, Sections 2 and 3, 5th Edition, McGraw-Hill Book Company, NY, 1973.

19. Reid, R.C., Prausnitz, J.M. and Sherwood, T.K., The properties of gases and liquids, 3rd Edition, McGraw-Hill Book Company, N.Y., 1977.

20. Rohsenow, W.M., A method of correlating heat transfer data for surface boiling of liquids, J. of Heat Transfer, Trans. ASME, C17, 4, pp 969, 1952.

21. Rohsenow, W.M., Nucleation with boiling heat transfer, ASME Paper No. 70-HT-18, 11 pages, 1970.

22. Shoukri, M., and Judd, R.L., On the influence of surface conditions in nucleate boiling - the concept of bubble flux density, J. of Heat Transfer, Trans. ASME, 100, 4, pp 618-623, 1978.

23. Singh, A., Mikic, B.B., and Rohsenow, W.M., Active sites in boiling, J. of Heat Transfer, Trans. ASME, C98, 3, pp 401-406, 1976.

24. Shoukri, M., and Judd, R.L., Nucleation Site Activation in Saturated Boiling, J. of Heat Transfer, Trans. ASME, 97,1, pp 93-98, 1975.

APPENDIX A

PROPERTY DATA

The property data at the Boiling points were calculated as follows :

1. The density of a pure liquid, ρ_1 , at the B.P. was calculated (within $\pm$ 3 percent) using Benson's equation (Perry and Chilton, 1973)

$$\rho_1 = \rho_c (1.981 + 0.422 \log p_c) \qquad (A.1)$$

where

ρ_c = liquid density at the critical point in g-mol cm^{-3}

p_c = critical pressure of the liquid in atmospheres absolute

The liquid density was also calculated using Tyn and Calus method (Reid et al. 1977).

The method is used for estimating liquid molal volumes, V_b, at B.P.

$$V_b = 0.285\ V_c^{1.048} \qquad (A.2)$$

where V_c = critical volume in cm^3 $g\text{-}mol^{-1}$, taken from the Property Data Bank of Reid et al. (1977).

2. The density of the vapor, ρ_v, was calculated using the Ideal gas equation at the normal B.P. and atmospheric pressure.

$$\rho_v = \frac{p}{RT} \qquad (A.3)$$

where p = atmospheric pressure, 1 atm

T = temperature, K

R = universal gas constant = 82.04 J kg-mol^{-1} K^{-1}

3. The dynamic viscosity of a pure liquid, μ_1 at the normal B.P. was determined using the equation suggested by Van Velzen, Cardozo and Langenkamp's method (Reid et al., 1977).

$$\log \mu_1 = \text{VISB}\left(\frac{1}{T} - \frac{1}{\text{VISTO}}\right) \qquad (A.4)$$

where,

VISB, VISTO = constants related to structure obtainable from the Data Bank of Reid et al.

T = temperature, K

μ_1 = viscosity, centipoise.

4. The surface tension, σ, at the normal B.P. was estimated within ≈ 5 percent using Walden's rule (Perry and Chilton, 1973)

$$\sigma = \frac{h_{fg}\rho_1}{364} \qquad (A.5)$$

where σ = surface tension, dynes cm^{-1}

h_{fg} = entholpy of vaporization, cal $g\text{-}mol^{-1}$

ρ_1 = liquid density, g cm^{-3}

5. The thermal conductivity of a pure liquid, k_1 , at the normal B.P. was established using Sato's correlation given in (Reid et al., 1977).

$$k_1 = \frac{2.64 \times 10^{-3}}{M^{1/2}} \qquad (A.6)$$

where

k_1 = thermal conductivity, cal cm^{-1} s^{-1} K^{-1}

M = molecular weight

6. The liquid specific heat, c_1, of Pentane and Ether at their B.P. was estimated using Missenard's group contribution method (Reid et al. 1977). The actual values at the B.P. were calculated using linear interpolation from the available data.

Properties of some pure liquids at Normal B.P.

Liquid	Molecular weight M	Normal Boiling point T_s K	Liquid Density $kg.m^{-3}$	Density of the v $kg.m^{-3}$	Enthalpy of vaporization $h_{fg} \times 10^{-5}$ $J.kg^{-1}$	Liquid viscosity $\mu \times 10^{4}$ $kg.s^{-1}m^{-1}$	Surface Tension $\sigma \times 10^{3}$ $kg.s^{-2}$	Liquid Thermal conductivity k $W.m^{-1}.K^{-1}$	Liquid specific heat c $J.kg^{-1}.K^{-1}$
Water	18.016	373.15	958.40	0.600	22.500	2.800	58.700	0.6825	4216
Pentane	72.150	309.22	622.20	2.844	3.573	1.974	11.273	0.1300	2333
Ether	74.120	307.66	697.60	2.937	3.510	1.971	13.310	0.1282	2495
Isopropanol	60.096	355.40	733.89	2.060	6.638	4.820	19.190	0.1425	3071
Benzene	78.120	353.25	811.85	2.700	3.940	3.290	19.800	0.0832	1956

APPENDIX B

DIMENSIONS OF VARIABLES USED IN CHAPTER 3

The dimensions in M,L,T,θ system are given below :

$[\delta] = L$

$[\dot{q}] = MLT^{-2}$

$[T_w - T_s] = \theta$

$[\rho_v] = ML^{-3}$

$[\rho_1] = ML^{-3}$

$[h_{fg}] = L^2T^{-2}$

$[\sigma] = MT^{-2}$

$[D_c] = L$

$[\mu_1] = ML^{-1}T^{-1}$

$[k_1] = MLT^{-3}\theta^{-1}$

$[c_1] = L^2T^{-2}\theta^{-1}$

$[S_R] = L$

APPENDIX C

SOLUTION OF FIRST ORDER ORDINARY DIFFERENTIAL EQUATIONS

The system of ODE's developed in Chapter 4 were solved numerically using the NAG Fortran Routine D02BDF (X,XEND,N,Y, TOL,IRELAB,FCN,STIFF,YNORM,W,IW,M,OUTPUT,IFAIL).

PARAMETERS :

X - initial value of the independent variable T

XEND - final value of the independent variable

N - number of equations

Y - array of dimension N

Y(1), Y(2), ..., Y(N) must contain the initial values

TOL - tolerance for error control

IRELAB - determines the type of error control

= 1 for number of correct decimal places

= 2 for number of correct significant digits

= 0 mixed error test

FCN - subroutine for evaluating functions.

It should be provided by the user and be of the type

SUBROUTINE FCN(T,Y,F)

DIMENSION T,Y(N), F(N)

FCN must be declared as EXTERNAL in the calling program.

STIFF - For stiffness check

= 0 no stiffness check is made

>0.0 stiffness value is computed at the end of each integration step

< 0.0 only the first stiffness value is calculated

YNORM - If YNORM = 0.0 then it has no effect

> 0.0 used as a bound on the computed solution

W - array of DIMENSION (N, IW) used partly for output and partly for workspace

IW - second dimension of W, $\geq$ 14

M - to call routine OUTPUT every M integration steps

OUTPUT - subroutine used to print the values of its arguments. It should be supplied by the user and be of the type SUBROUTINE OUTPUT (X,Y,W,STIFF)
OUTPUT must be declared as EXTERNAL in the calling program.

IFAIL - error indicator.

APPENDIX D

CONVECTIVE HEAT TRANSFER COEFFICIENTS

The adjusted values of the convective heat transfer coefficients h_{ic} and h_{wli} were determined using the following equations

$$h_{ic} = h_i \, M_1 \tag{D.1}$$

$$h_{wli} = h_w \, M_2 \tag{D.2}$$

The interfacial coefficient, h_i, was determined from an expression based upon the kinetic theory of gases (Kant, 1983, equation (A4.4)) as

$$h_i = \left(\frac{h_{fg} \, p_v}{T_v}\right) \left(\frac{M}{2\pi R T_v}\right)^{1/2} \left[\left(\frac{h_{fg} \, M}{R \, T_v}\right) - 0.5\right] \tag{D.3}$$

The coefficient, h_w, was taken as the heat transfer coefficient for the laminar fully developed flow of a fluid through a tube, for constant wall temperature, given by

$$h_w = 3.658 \, (k_1/D_c) \tag{D.4}$$

Other symbols have their usual meanings.